

NBI-98-21

UALG/TP/98-6

September 1998

Non-perturbative computation of gluon mini-jet production in nuclear collisions at very high energies

Alex Krasnitz

UCEH, Universidade do Algarve Campus de Gambelas, P-8000 Faro, Portugal

Raju Venugopalan

Niels Bohr Institute, Blegdamsvej 17, Copenhagen, Denmark, DK-2100

Abstract

At very high energies, in the infinite momentum frame and in light cone gauge, a hard scale proportional to the high parton density arises in QCD. In an effective theory of QCD at small x , this scale is of order $\alpha_S \mu$, where μ is simply related to the gluon density at higher rapidities. The *ab initio* real time evolution of small x modes in a nuclear collision can be described consistently in the classical effective theory and various features of interest can be studied non-perturbatively. In this paper, we discuss results from a real time SU(2) lattice computation of the production of gluon jets at very high energies. At very large transverse momenta, $k_t \geq \mu$, our results match the predictions from pQCD based mini-jet calculations. Novel non-perturbative behaviour of the small x modes is seen at smaller momenta $k_t \sim \alpha_S \mu$. Gauge invariant energy-energy correlators are used to estimate energy distributions evolving in proper time.

1 Introduction

It is of considerable theoretical and experimental interest to understand the collisions of nuclei at ultrarelativistic energies and the putative evolution of the hot and dense matter created in these collisions into a thermalized, deconfined state of matter called a quark gluon plasma. The theoretical challenge is to understand the dynamics of the formation of this matter and its properties from QCD while the experimental challenge is to detect evidence that such a plasma was indeed formed [1].

The space–time evolution of the nuclei after the collision and the magnitudes and relevance of various proposed signatures of this hot and dense matter depend sensitively on the initial conditions for the evolution, namely, the parton distributions in each of the nuclei *prior* to the collision. In the standard perturbative QCD approach to the problem, observables from the collision may be computed by convolving the parton distributions of each nucleus, determined from deep inelastic scattering experiments, with the elementary parton–parton scattering cross sections. At the high energies of the RHIC and LHC colliders, hundreds of mini–jets may be formed in the initial collision [2, 3, 4]. The final state interactions of these mini–jets are often described in multiple scattering Glauber–Gribov models (see Ref. [5] and references therein) or in classical cascade approaches to obtain the space–time evolution (see Ref. [6] and references therein). The possible “quenching” of these mini–jets has also been studied and proposed as a signature of the formation of a quark gluon plasma [7]. Recently, initial conditions for the energy density and velocity obtained in the mini–jet approach have been used in a simple hydrodynamic model to study the late time evolution of matter in high energy nuclear collisions [8, 9].

While the above “probabilistic” approach provides a reasonable description of large transverse momentum processes at large x , QCD coherence effects become important as we go to small x or alternatively, towards central rapidities [10]. This is because small x partons in one nucleus may “see” more than one parton in the

direction of the incoming nucleus resulting in a breakdown of the above described convolution of distributions. What is needed therefore to describe the collision of the “wee” nuclear partons is a wave picture where coherent multiple scattering is fully taken into account.

At what values of x would this picture become applicable? Strictly speaking, coherence or shadowing effects start to become important when wee partons from neighbouring nucleons overlap, i.e., when $x < 1/(2R_N m_N) \approx 0.1$ fm. Here R_N denotes the nucleon radius and m_N the nucleon mass. However, several authors have shown that with an appropriate choice of the non-perturbative input structure functions, the standard leading twist perturbative evolution equations still work fairly well in the shadowing region below $x = 0.1$ [11, 12]. To determine at precisely what value of x coherence effects become large one needs to compute the two gluon distribution function at small x . Following the pioneering work of Gribov, Levin and Ryskin [13] and of Mueller and Qiu [14], there has been a considerable body of recent work directed towards addressing this issue [20, 19, 15].

In this paper, we will describe an *ab initio* QCD based effective theory approach to the theoretical study of nuclear collisions at very high energies. This model of high energy nuclear collisions naturally incorporates coherence effects which become important at small x and small transverse momenta while reproducing simultaneously the standard mini-jet results at large transverse momenta. It has the further advantage of containing a self-consistent space-time picture of the nuclear collision. The model is based on an effective action approach to QCD initially developed by McLerran and Venugopalan [16], and later further developed by Ayala, Jalilian-Marian, McLerran and Venugopalan [17], and by J.Jalilian-Marian, Kovner, McLerran, Leonidov and Weigert [18, 19, 20].

The above mentioned effective action contains one dimensionful parameter, $\chi(y, Q^2)$. (This parameter is also often used interchangeably with μ in the text; the distinction between the two is discussed in section 3.) Here χ is the total color charge squared

per unit area integrated from the rapidity y of interest to the beam rapidity. It is the only scale in the problem and we expect therefore that the coupling constant runs as a function of this scale. One therefore has weak coupling in the limits where the color charge χ is large; either for $A \gg 1$ or $s \rightarrow \infty$. It was argued that the classical fields corresponding to the saddle point solutions of the effective theory are the non-Abelian analogue of the Weizsäcker-Williams fields in classical electrodynamics. Exact analytical expressions for these fields have been obtained recently [18, 21]. Further, it has been shown explicitly that χ obeys renormalization group equations in y and Q^2 . These reduce to the well known BFKL and DGLAP equations respectively [22] in the appropriate limits [19, 20].

The above model was first applied to the problem of nuclear collisions by Kovner, McLerran and Weigert, who formulated the problem as the collision of Weizsäcker-Williams fields [23]. The classical fields after the collision then correspond to solutions of the Yang-Mills equations in the presence of static, random sources of color charge on the light cone. The initial conditions for the dynamical evolution of the small x modes of the two nuclei after the collision were formulated and perturbative solutions obtained for modes with transverse momenta $k_t \gg \alpha_S \sqrt{\chi}$. After averaging over the Gaussian random sources of color charge on the light cone, the energy and number distributions of physical gluons were computed. Further, the classical gluon radiation from these perturbative modes was studied by these authors and later in greater detail by several others [24, 25, 26]. In the small x limit, it was shown that the classical Yang-Mills result agreed with the quantum Bremsstrahlung result of Gunion and Bertsch [29].

While the perturbative approach is very relevant and useful, it is still essential to consider the full non-perturbative approach for the following reasons. Firstly, the classical gluon radiation computed perturbatively is infrared singular and has to be cut-off at some scale. This problem also arises in mini-jet calculations where at high energies results are shown to be rather sensitive to the cut-off [9]. It was argued in

Ref. [23, 25] that a natural scale where the distributions are cut-off is given by $k_t \sim \alpha_S \sqrt{\chi}$. However, since quantitative differences can be large, it is important to perform a full calculation. Secondly, the non-perturbative approach is crucial to study the space-time evolution of the nuclei and in particular, the possible thermalization of the system and the relevant time scales for thermalization. This in turn has several ramifications for computations of various signatures of the quark gluon plasma. For instance, if thermalization does occur, then as proposed by Bjorken [27] hydrodynamic evolution of the system is reasonable. In that event, our approach would provide the initial temperature and velocity profiles necessary for such an evolution [8] (see also [28] and references therein).

We discuss in this paper results from real time simulations of the full, non-perturbative evolution of classical non-Abelian Weizsäcker-Williams fields. Such a simulation is possible since the fields are classical. Similar simulations of the real time evolution of classical fields have been performed in the context of sphaleron-mediated baryon number violation [30] and chirality violating transitions in hot gauge theories [31].

In brief, the idea is as follows [32]. We write down the lattice Hamiltonian which describes the evolution of the small x classical gauge fields. It is the Kogut-Susskind Hamiltonian in 2+1-dimensions coupled to an adjoint scalar field. For simplicity, we restrict our study in this paper to an SU(2) gauge theory. The extension to the physical SU(3) case will be considered at a later date. The lattice equations of motion for the fields are determined straightforwardly using Hamilton's equations. The initial conditions for the evolution are provided by the Weizsäcker-Williams fields for the nuclei before the collisions. Interestingly, the dependence on the static light cone sources does not enter through the Hamiltonian but instead from the initial conditions. Also, to reiterate, our results have to be averaged over by the above mentioned Gaussian measure for each source.

A limitation of our approach is that it is classical-quantum fluctuations have been

neglected. However if the effective action approach captures the essential physics of the small x modes of interest, then in the spirit of the Wilson renormalization group, quantum information from the large x modes (above the rapidity of interest) is contained in the parameter $\chi(y, Q^2)$ discussed above, which grows rapidly as one goes to smaller and smaller x 's. This information can be included in the classical lattice simulations. Thus as long as we are not at small enough x where the above picture of Gaussian random sources breaks down, the residual quantum fluctuations about the classical saddle point of the effective theory should be small and the above classical picture of nuclear collisions should be valid ¹.

A related approach is that of Mueller, Kovchegov and Wallon [33, 34], where they combined Mueller's dipole picture of high energy scattering [35, 36] with the classical Yang–Mills picture [21] to study nucleon–nucleus scattering. In particular, Mueller and Kovchegov make the interesting observation in their calculation of nucleon–nucleus scattering that, in light cone gauge, the effect of final state interactions is already contained in the wavefunction of the incoming hadron. This observation is very much at the heart of this work because what final state interactions there are, are very much determined by the initial conditions given by the small x wavefunctions of the nuclei before the collision. For alternative approaches, we refer the reader to the work of Makhlin and Surdutovich [37] and that of Balitskii [38].

Our paper is organized as follows. In the following section we discuss the problem of initial conditions for nuclear collisions as formulated by Kovner, McLerran and Weigert and their perturbative solutions of the Yang–Mills equations and computation of gluon production in this approach. We discuss a non–perturbative Hamiltonian approach to the solution of the full Yang–Mills equations.

¹The classical picture of nuclear collisions will also be valid at very small x but the Gaussian weight with which we average over the classical configurations will change. The functional replacing the Gaussian weight is the solution of a non–linear renormalization group equation [20] and is yet to be determined.

In section 3, we formulate the problem of solving the Yang–Mills equations on the lattice. Assuming boost invariance and $N_c = 2$, we write down the lattice action in 2+1–dimensions. The lattice action is used to construct the lattice analog of the continuum initial conditions. This is done by matching the singular pieces of the lattice equations of motion on the light cone. Once the initial conditions are determined, we write down the lattice Hamiltonian and the equations of motion for the evolution of the dynamical fields and their conjugate momenta in the forward light cone.

In section 4, we use lattice perturbation theory to relate the parameters of our lattice calculation, such as the parameter proportional to the parton density, μ , the lattice size L and the lattice time τ , to physical strong interaction scales. We also discuss the relation of gauge invariant quantities computed on the lattice to experimental observables that might be measured in heavy ion collisions at RHIC and LHC.

Numerical results from our simulations are discussed in section 5. These are performed for a range of values of $g^2\mu = 0.018$ – 0.2 , and for lattice sizes from 10×10 to 160×160 , both measured in units of the lattice spacing. (We will assume boost invariance throughout, which simplifies our simulation to a 2–dimensional one.) We first compare the field intensities and the time evolution of hard modes in the collision with the predictions of lattice perturbation theory and find excellent agreement. Significant deviations from lattice perturbation theory are found for the softer modes $k_t \sim \alpha_S\mu$, particularly at larger values of μ . We study the dependence of our results on the lattice size. We demonstrate the behaviour of the chromo–electric and chromo–magnetic fields as a function of time and that of those components of the stress energy tensor that may be related to experimental observables.

We summarize our results in section 6 and discuss further computations that may be performed in this approach. There are two appendices. The first appendix discusses our numerical algorithm and procedure. The second is a derivation of the

lattice perturbation theory expressions for the field intensity and the kinetic energy at $\tau = 0$. These expressions were compared to the full lattice results at large transverse momenta.

2 Classical gluon radiation in high energy nuclear collisions

In the work of McLerran and Venugopalan [16], the classical gluon field at small x for a nucleus in the infinite frame is obtained by solving the Yang–Mills equations in the presence of a static source of color charge $\rho^a(r_t, \eta)$ on the light cone. This corresponds to the saddle point solution of their small x effective action. Exact solutions for the classical field as functions of $\rho^a(r_t, \eta)$ were found by Jalilian–Marian et al. [18] and independently by Kovchegov [21]. Distribution functions are computed by averaging products of the classical fields over a Gaussian measure in ρ with the variance $\mu^2(\eta, Q^2)$. Here μ^2 is the color charge squared per unit area per unit rapidity resolved at a scale Q^2 by an external probe. It is related to χ by the expression

$$\chi(\eta, Q^2) = \int_{\eta}^{\infty} d\eta' \mu^2(\eta', Q^2). \quad (1)$$

The above picture of gluon fields in a nucleus at small x was extended to describe nuclear collisions by Kovner, McLerran and Weigert [23].

In this section, we shall discuss their formulation of the problem in the *continuum* and their perturbative computation, to second order in the parameter $\alpha_S \mu/k_t$, of classical gluon radiation in nuclear collisions. (Readers familiar with the discussion in Refs. [23]–[26] can skip sections 2.1 and 2.2 and go directly to 2.3.) In section 2.3 we then briefly discuss a non–perturbative Hamiltonian approach which suggests how all orders in $\alpha_S \mu/k_t$ can be computed numerically. The implementation of this approach on the lattice is described in section 3.

2.1 The non-Abelian Weizsäcker-Williams approach to high energy nuclear collisions

In nuclear collisions at very high energies, the hard valence parton modes act as highly Lorentz contracted, static sources of color charge for the wee parton, Weizsäcker-Williams modes in the nuclei. The sources are described by the current

$$J^{\nu,a}(r_t) = \delta^{\nu+} \rho_1^a(r_t) \delta(x^-) + \delta^{\nu-} \rho_2^a(r_t) \delta(x^+), \quad (2)$$

where ρ_1 and ρ_2 correspond to the color charge densities of the hard modes in nucleus 1 and nucleus 2 respectively. The classical field of two nuclei describing the wee parton dynamics is given by the solutions of the Yang-Mills equations in the presence of two light cone sources. We have then

$$D_\mu F^{\mu\nu} = J^\nu. \quad (3)$$

Gluon distributions are simply related to the Fourier transform $A_i^a(k_t)$ of the solution to the above equation by $\langle A_i^a(k_t) A_i^a(k_t) \rangle_\rho$. The averaging over the classical charge distributions is defined by

$$\begin{aligned} \langle O \rangle_\rho &= \int d\rho_1 d\rho_2 O(\rho_1, \rho_2) \\ &\times \exp\left(-\int d^2r_t \frac{\text{Tr}[\rho_1^2(r_t) + \rho_2^2(r_t)]}{2g^4\mu^2}\right). \end{aligned} \quad (4)$$

The averaging over the color charge distributions is performed independently for each nucleus with equal Gaussian weight $g^4\mu^2$. (Note that this is only true for the case of identical nuclei which will be assumed implicitly throughout the rest of this paper.)

The observant reader will notice that we have omitted the rapidity dependence of the the charge distributions in the equations immediately above. We will justify this omission in our discussion of the lattice Hamiltonian. We note that the rapidity dependence of the charge distribution is also absent in Ref. [23] (see the discussion below Eq. 10).

Before the nuclei collide ($t < 0$), a solution of the equations of motion is

$$\begin{aligned} A^\pm &= 0, \\ A^i &= \theta(x^-)\theta(-x^+)\alpha_1^i(r_t) + \theta(x^+)\theta(-x^-)\alpha_2^i(r_t), \end{aligned} \quad (5)$$

where $\alpha_q^i(r_t)$ ($q = 1, 2$ denote the labels of the nuclei) are pure gauge fields defined through the gauge transformation parameters $\Lambda_q(\eta, r_t)$ [24]

$$\alpha_q^i(r_t) = \frac{1}{i} \left(P e^{-i \int_{\pm\eta_{\text{proj}}}^0 d\eta' \Lambda_q(\eta', r_t)} \right) \nabla^i \left(P e^{i \int_{\pm\eta_{\text{proj}}}^0 d\eta' \Lambda_q(\eta', r_t)} \right)^\dagger. \quad (6)$$

Here $\eta = \eta_{\text{proj}} - \log(x^-/x_{\text{proj}}^-)$ is the rapidity of the nucleus moving along the positive light cone with the gluon field α_1^i and $\eta = -\eta_{\text{proj}} + \log(x_{\text{proj}}^+/x^+)$ is the rapidity of the nucleus moving along the negative light cone with the gluon field α_2^i . The $\Lambda_q(\eta, r_t)$ parameters are, in turn, determined by the color charge distributions:

$$\Delta_\perp \Lambda_q = \rho_q; \quad q = 1, 2 \quad (7)$$

Δ_\perp being the Laplacian in the perpendicular plane.

It is expected that at central rapidities (or $x \ll 1$) the source density varies slowly as a function of rapidity and $\alpha^i \equiv \alpha^i(r_t)$. The above expression suggests that for $t < 0$ the solution is simply the sum of two disconnected pure gauges. Just as in the Weizsäcker–Williams limit in QED, the transverse components of the electric field are highly singular.

For $t > 0$ the solution is no longer pure gauge. Working in the Schwinger gauge

$$x^+ A^- + x^- A^+ = 0, \quad (8)$$

or $A^\tau = 0$, the authors of Ref. [23] found that with the ansatz

$$\begin{aligned} A^\pm &= \pm x^\pm \alpha(\tau, r_t), \\ A^i &= \alpha_\perp^i(\tau, r_t), \end{aligned} \quad (9)$$

where $\tau = \sqrt{2x^+x^-}$, Eq. 3 could be written in the simpler form

$$\begin{aligned}
\frac{1}{\tau^3}\partial_\tau\tau^3\partial_\tau\alpha + [D_i, [D^i, \alpha]] &= 0, \\
\frac{1}{\tau}[D_i, \partial_\tau\alpha_\perp^i] + i\tau[\alpha, \partial_\tau\alpha] &= 0, \\
\frac{1}{\tau}\partial_\tau\tau\partial_\tau\alpha_\perp^i - i\tau^2[\alpha, [D^i, \alpha]] - [D^j, F^{ji}] &= 0.
\end{aligned} \tag{10}$$

Note that the above equations of motion are independent of η —the gauge fields in the forward light cone are therefore only functions of τ and r_t and are explicitly boost invariant. We will use this fact later in our discussion of the Hamiltonian approach.

The initial conditions for the fields $\alpha(\tau, r_t)$ and α_\perp^i at $\tau = 0$ are obtained by matching the equations of motion (Eq. 3) at the point $x^\pm = 0$ and along the boundaries $x^+ = 0, x^- > 0$ and $x^- = 0, x^+ > 0$. Because the sources are highly singular functions along their respective light cones, so too in general will be the equations of motion. Remarkably, however, there exists a set of non-singular initial conditions that ensure the smooth evolution of the classical fields in the forward light cone. These are obtained by matching the singular terms in the equations of motion before and after the collision at $\tau = 0$. In terms of the fields of each of the nuclei before the collision ($t < 0$), the fields after the collision ($t > 0$) are

$$\begin{aligned}
\alpha_\perp^i|_{\tau=0} &= \alpha_1^i + \alpha_2^i, \\
\alpha|_{\tau=0} &= \frac{i}{2}[\alpha_1^i, \alpha_2^i].
\end{aligned} \tag{11}$$

Gyulassy and McLerran have shown [24] that even when the fields $\alpha_{1,2}^i$ before the collision are smeared out in rapidity to properly account for singular contact terms in the equations of motion the above boundary conditions remain unchanged. Further, since the equations are very singular at $\tau = 0$, the only condition on the derivatives of the fields that would lead to regular solutions are $\partial_\tau\alpha|_{\tau=0}, \partial_\tau\alpha_\perp^i|_{\tau=0} = 0$.

2.2 Review of perturbative solution of the Yang–Mills equations

In Ref. [23], perturbative solutions (for small ρ) were found to order ρ^2 by expanding the initial conditions and the fields in powers ρ (or equivalently, in powers of $\alpha_S\mu/k_t$) as

$$\alpha = \sum_{n=0}^{\infty} \alpha_{(n)} ; \alpha_{\perp}^i = \sum_{n=0}^{\infty} \alpha_{\perp(n)}^i , \quad (12)$$

where the subscript n denotes the n th order in ρ . Since it is relevant to the discussion in the following sections (particularly appendix B) , we outline their solution below with a commentary but refer the reader to their paper for the details.

To lowest order in ρ , the Yang–Mills equations of motion are linear in $\alpha_{(1)}$ and $\alpha_{\perp(1)}^i$. The solution is the trivial Abelian solution

$$\alpha_{(1)} = 0 ; \alpha_{\perp(1)}^i = -\partial^i(\phi^1 + \phi^2)(x_t) , \quad (13)$$

where $\phi^a = \frac{-1}{\nabla_{\perp}^2}\rho^a$. Clearly $\alpha_{\perp(1)}$ above is a pure gauge. To second order in ρ , the equations of motion are nearly homogeneous except for a non–linear term proportional to $[\alpha_{\perp(1)}^j, \alpha_{\perp(1)}^i]$ in the equation for $\alpha_{\perp(2)}^i$. This piece can be removed from the equations of motion to this order by making use of the residual, τ –independent gauge transformation $A_{\mu} = V(x_t)[\epsilon_{\mu} - \frac{1}{i}\partial_{\mu}] V^{\dagger}(x_t)$ and fixing V such that ϵ^i satisfies the two dimensional Coulomb gauge condition $\partial^i\epsilon^i|_{\tau=0} = 0$. As described in appendix B, the lattice Coulomb gauge condition is fixed in an analogous way to eliminate the residual gauge freedom on the lattice.

Writing $\epsilon^i = \epsilon^{ij}\partial^j\chi$, where ϵ^{ij} is the two dimensional anti–symmetric Levi–Civita tensor, the Yang–Mills equations in the forward light cone (Eq. 10) may be written as

$$\begin{aligned} \frac{1}{\tau^3}\partial_{\tau}\tau^3\partial_{\tau}\epsilon_{(2)} - \nabla_{\perp}^2\epsilon_{(2)} &= 0 , \\ \frac{1}{\tau}\partial_{\tau}\tau\partial_{\tau}\chi_{(2)} - \nabla_{\perp}^2\chi_{(2)} &= 0 . \end{aligned} \quad (14)$$

with the initial conditions

$$\begin{aligned}\epsilon_{(2)}|_{\tau=0} &= \frac{i}{2}[\partial^i \phi^1, \partial^i \phi^2], \\ \chi_{(2)}|_{\tau=0} &= -i\epsilon^{ij}[\partial^i \phi^1, \partial^j \phi^2].\end{aligned}\tag{15}$$

The residual Coulomb gauge fixing at this second order therefore shifts the nonlinearities from the equations of motion to the initial conditions.

The solutions of Eqs. 14 can be written in terms of Bessel functions as

$$\begin{aligned}\epsilon_{(2)}(\tau, x_t) &= \int \frac{d^2 k_t d^2 y_t}{(2\pi)^2} e^{ik_t \cdot (x-y)_t} h_3(y_t) \frac{1}{\omega\tau} J_1(\omega\tau), \\ \chi_{(2)}(\tau, x_t) &= \int \frac{d^2 k_t d^2 y_t}{(2\pi)^2} e^{ik_t \cdot (x-y)_t} h_1(y_t) J_0(\omega\tau),\end{aligned}\tag{16}$$

where

$$\begin{aligned}h_3(y_t) &= i[\partial^i \phi^1, \partial^i \phi^2](y_t), \\ h_1(y_t) &= -i\epsilon^{ij} \frac{1}{\nabla_{\perp}^2} [\partial^i \phi^1, \partial^j \phi^2](y_t).\end{aligned}\tag{17}$$

Here $\omega = |k_t|$. Note that in the solutions to the gauge fields above, the spatial and temporal distributions factorize. The amplitudes of the fields in this perturbative approach are therefore completely determined at $\tau = 0$. In section 5, we will see that in weak coupling the large transverse momentum modes show the above Bessel behavior. (In lattice perturbation theory, the form is the same as above. The difference is that ω obeys a lattice dispersion relation).

At late times $\omega\tau \gg 1$, the well known asymptotic expressions for the Bessel functions can be used to write the solutions in Eq. 16 as

$$\begin{aligned}\epsilon_{(2)}(\tau, x_t) &= \int \frac{d^2 k_t}{(2\pi)^2} \frac{1}{\sqrt{2\omega}} \left\{ a_1(\vec{k}_t) \frac{1}{\tau^{3/2}} e^{ik_t \cdot x_t - i\omega\tau} + h.c. \right\}, \\ \epsilon^i(\tau, x_t) &= \int \frac{d^2 k_t}{(2\pi)^2} \kappa^i \frac{1}{\sqrt{2\omega}} \left\{ a_2(\vec{k}_t) \frac{1}{\tau^{1/2}} e^{ik_t \cdot x_t - i\omega\tau} + h.c. \right\}.\end{aligned}\tag{18}$$

Here $\kappa^i = \epsilon^{ij} k_t^j / \omega$ and

$$a_1(k_t) = \frac{1}{\sqrt{\pi}} \frac{h_3(k_t)}{\omega}; \quad a_2(k_t) = \frac{1}{\sqrt{\pi}} i\omega h_1(k_t),\tag{19}$$

where h_1 and h_3 are now the Fourier transforms of Eq. 17.

The energy distribution in a transverse box of size R and longitudinal extent dz can be computed by summing over the energy of the modes in the box with the occupation number of the modes given by the functions $a_i(k_t)$ above. We have then (for $\omega\tau \gg 1$)

$$\frac{dE}{dyd^2k_t} = \frac{1}{(2\pi)^2} \sum_{i,b} |a_i^b(k_t)|^2. \quad (20)$$

The multiplicity distribution of classical gluons is defined as $dE/dyd^2k_t/\omega$. After performing the averaging over the Gaussian sources, the number distribution of classical gluons is

$$\frac{dN}{dyd^2k_t} = \pi R^2 \frac{2g^6 \mu^4}{(2\pi)^4} \frac{N_c(N_c^2 - 1)}{k_t^4} L(k_t, \lambda), \quad (21)$$

where $L(k_t, \lambda)$ is an infrared divergent function at the scale λ . It will be discussed further below. We first note that this result agrees with the quantum bremsstrahlung formula of Gunion and Bertsch [29] and with several later works [24, 25, 26]. It was also shown by Gyulassy and McLerran that when the sources are smeared in rapidity, the expression that results is identical to the one above except $\mu^4 \rightarrow \chi^+(y)\chi^-(y)$ where the \pm superscripts refer to the nucleus on the positive or negative light cone respectively.

The origin of the infrared divergent function $L(k_t, \lambda)$ above is from long range color correlations which are cut-off either by a nuclear form factor (as in Refs. [29, 25]), by dynamical screening effects [39, 40] or in the classical Yang–Mills case of Ref. [23], non-linearities that become large at the scale $k_t \sim \alpha_S \mu$. In the classical case then,

$$L(k_t, \lambda) = \log(k_t^2/\lambda^2), \quad (22)$$

where $\lambda = \alpha_S \mu$. A similar logarithmic behaviour at small transverse momenta can be deduced from the dipole form factors used in Refs. [29, 39]. A power law ($\sim 1/k_t^2$) infrared behaviour is predicted in Ref. [25]. The formalism used in all these derivations

breaks down at small momenta and one cannot distinguish between the different parametrizations of the nuclear form factors. However, at sufficiently high energies, the behaviour of $L(k_t, \lambda)$ in the infrared is given by higher order (in $\alpha_S \mu / k_t$) non-linear terms in the classical effective theory. One of the goals of our work is to address precisely this question: how do non-perturbative effects in the classical effective theory change the gluon distributions at small transverse momenta?

2.3 The Hamiltonian approach

While the Yang–Mills equations can be solved perturbatively, in the limit $\alpha_S \mu \ll k_t$, it is unlikely that a simple analytical solution exists for Eq. 3 in the non-perturbative regime where $k_t \leq \mu$. The classical solutions have to be determined numerically for $t > 0$. The straightforward procedure would be to discretize Eq. 3. It will be more convenient for our purposes though to construct the lattice Hamiltonian and obtain the lattice equations of motion from Hamilton’s equations. This will be done in the next section. Before we do that, we will discuss here the form of the continuum Hamiltonian and comment on our assumption of boost invariance.

We start from the QCD action (without dynamical quarks)

$$S_{QCD} = \int d^4x \sqrt{-g} \left\{ \frac{1}{4} g^{\mu\lambda} g^{\nu\sigma} F_{\mu\nu} F_{\lambda\sigma} - j^\mu A_\mu \right\}, \quad (23)$$

where $g = \det(g_{\mu\nu})$. In the forward light cone ($t > 0$) it is convenient to work with the τ, η, \vec{r}_t co-ordinates where $\tau = \sqrt{2x^+x^-}$ is the proper time, $\eta = \frac{1}{2} \log(x^+/x^-)$ is the space-time rapidity and $\vec{r}_t = (x, y)$ are the two transverse Euclidean co-ordinates. In these co-ordinates, the metric is diagonal with $g^{\tau\tau} = -g^{xx} = -g^{yy} = 1$ and $g^{\eta\eta} = -1/\tau^2$.

After a little algebra, the Hamiltonian can be written as [41]

$$H = \tau \int d\eta d^2r_t \left\{ \frac{1}{2} p^{\eta,a} p^{\eta,a} + \frac{1}{2\tau^2} p^{r,a} p^{r,a} + \frac{1}{2\tau^2} F_{\eta r}^a F_{\eta r}^a + \frac{1}{4} F_{ij}^a F_{ij}^a + j^{\eta,a} A_\eta^a + j^{r,a} A_r^a \right\}. \quad (24)$$

Here we have adopted the gauge condition of Eq. 8, which is equivalent to requiring $A^\tau = 0$. Also, $p^\eta = \frac{1}{\tau} \partial_\tau A_\eta$ and $p^r = \tau \partial_\tau A_r$ are the conjugate momenta.

Consider the field strength $F_{\eta r}$ in the above Hamiltonian. If we assume approximate boost invariance, or

$$A_r(\tau, \eta, \vec{r}_t) \approx A_r(\tau, \vec{r}_t); \quad A_\eta(\tau, \eta, \vec{r}_t) \approx \Phi(\tau, \vec{r}_t), \quad (25)$$

we obtain

$$F_{\eta r}^a = -D_r \Phi^a, \quad (26)$$

where $D_r = \partial_r - igA_r$ is the covariant derivative. Further, if we express $j^{\eta, r}$ in terms of the j^\pm defined in Eq. 2 we obtain the result that $j^{\eta, r} = 0$ for $\tau > 0$.

Performing the integration over the space-time rapidity, we can re-write the Hamiltonian in Eq. 24 as

$$H = \int d\vec{r}_t \eta \left\{ \frac{1}{2\tau} E_r^a E_r^a + \frac{\tau}{4} F_{ij}^a F_{ij}^a + \frac{1}{2\tau} (D_r \Phi)^a (D_r \Phi)^a + \frac{\tau}{2} p_\eta^a p_\eta^a \right\}. \quad (27)$$

We have thus succeeded in expressing the Hamiltonian in Eq. 24 as the Yang–Mills Hamiltonian in 2+1–dimensions coupled to an adjoint scalar. The discrete version of the above Hamiltonian is well known and is the Kogut–Susskind Hamiltonian [42] in 2+1–dimensions coupled to an adjoint scalar field. The lattice Hamiltonian will be discussed further in the next section.

We now comment on a key assumption in the above derivation, namely, the boost invariance of the fields. This invariance results in Eq. 27 thereby allowing us to restrict ourselves to a transverse lattice alone. To clarify the issue we are compelled to make a few historical remarks. As we mentioned earlier, the authors of Ref. [23] found a solution which was explicitly boost invariant. However, this result was a consequence of the original assumption of McLerran and Venugopalan that the color charge density factorizes, $\rho^a(r_t, \eta) \rightarrow \rho^a(r_t) \delta(x^-)$. It was noticed in Ref. [43] that this factorized form for the charge density results in infrared singular correlation functions which diverge

as the square of the lattice size. This problem was subsequently resolved in Ref. [18] where the authors realized that a rapidity dependent charge density $\rho^a(r_t, \eta)$ would give infrared safe solutions. This might be interpreted as implying that the boost invariance assumption of Ref. [23] should be given up as well.

Fortunately, this is not necessary. In principle, the rapidity dependence of the color charge density can be arbitrarily weak since that is sufficient to obtain infrared safe correlation functions. In Ref. [44], an explicit model was constructed for the color charge distribution in the fragmentation region. It was shown there that for $\eta < \eta_{\text{proj}}$ the color charge distribution had a very weak dependence on η . Further, as mentioned earlier, it was shown by Gyulassy and McLerran [24] that the initial conditions in Eq. 11 are unaffected by the smearing in rapidity.

In general, at the energies of interest, particle distributions are unlikely to be boost invariant. Eskola, Kajantie and Ruuskanen [8] have shown in the mini-jet picture that the final distributions are more like broad Gaussians. This would be true in our case as well since μ^2 is in general a function of the rapidity and this dependence may be strong in the central region. If we wish to describe particle distributions for a range of rapidities as opposed to our current restriction to 1 unit in rapidity, we will have to give up our assumption of boost invariance. This can be easily done, but it will be numerically more time consuming as well.

3 Real-time lattice description of nuclear collisions

In the previous section we discussed the continuum formulation of nuclear collisions in terms of collisions of non-Abelian Weizsäcker-Williams fields. The initial conditions for the evolution after the collision were obtained by requiring that the singular contributions to the equations of motion on the light cone vanish. We next discussed the perturbative solutions of the equations of motion for our choice of initial conditions and obtained a result for the number distribution of radiated gluons.

In this section, we will formulate the problem on the lattice. We begin by writing down the lattice action and equations of motion. From the lattice action, we can identify the singular terms in the lattice equations of motion. Matching these on the light cone uniquely gives us the initial conditions on the lattice. We end with a discussion of Hamilton's equations of motion for the evolution of dynamical fields on the lattice with the initial conditions specified at $\tau = 0$.

3.1 Lattice action and equations of motion

In this sub-section, we will write down the lattice action in 2+1-dimensions and the rules to derive the lattice equations of motion from this action. In the following sub-section, we will identify the singular terms in the lattice action and use these to derive the correct initial conditions for dynamical evolution of fields on the lattice for $\tau > 0$.

The action is defined in the 4-space discretized in the transverse directions, while z and t are continuous. The appropriate expression is derived starting from the Minkowski Wilson action in the discretized 4-space and taking the naive continuum limit in the longitudinal directions. The Minkowski Wilson action for the $SU(N_c)$ gauge group in fundamental representation reads

$$S = a^{-2} \sum_{zt} \left(1 - \frac{1}{N_c} \Re \text{Tr} U_{zt} \right) + \sum_{t\perp} \left(1 - \frac{1}{N_c} \Re \text{Tr} U_{t\perp} \right) - \sum_{z\perp} \left(1 - \frac{1}{N_c} \Re \text{Tr} U_{z\perp} \right) - a^2 \sum_{\perp} \left(1 - \frac{1}{N_c} \Re \text{Tr} U_{\perp} \right),$$

where zt , $z\perp$, $t\perp$ and \perp are, in obvious notation, plaquettes lying in various 2-planes of the 4-space and \Re denotes the real component. A plaquette is defined as

$$U_{jlm} \equiv U_{j,l} U_{j+l,m} U_{j+m,l}^\dagger U_{j,m}^\dagger.$$

where j is a site index and l, m are direction indices. We now take the formal continuum limit in the longitudinal directions by writing longitudinal links as $U =$

$\exp(iaA)$, letting $a \rightarrow 0$ and assuming that all the fields are smooth functions of longitudinal coordinates. The powers of a in front of various terms in S have been chosen with this formal limit in mind. Replacing $a^2 \sum_{zt}$ with $\int dzdt$, we then have for the action

$$S = \int dzdt \sum_{\perp} \left[\frac{1}{2N_c} \text{Tr} F_{zt}^2 + \frac{1}{N_c} \Re \text{Tr} (M_{t\perp} - M_{z\perp}) - \left(1 - \frac{1}{N_c} \Re \text{Tr} U_{\perp} \right) \right], \quad (28)$$

where

$$M_{t,jn} \equiv \frac{1}{2} (A_{t,j}^2 + A_{t,j+n}^2) - U_{j,n} \left[\frac{1}{2} \partial_t^2 U_{j,n}^{\dagger} + i (A_{t,j+n} \partial_t U_{j,n}^{\dagger} - \partial_t U_{j,n}^{\dagger} A_{t,j}) + A_{t,j+n} U_{j,n}^{\dagger} A_{t,j} \right], \quad (29)$$

and similarly for $M_{z,jn}$.

The equation of motion for a field is obtained by varying S with respect to that field. For the longitudinal fields $A_{t,z}$ the variation has the usual meaning of a partial derivative. For transverse link matrices U_{\perp} the variation amounts to a covariant derivative

$$D^{\gamma} S(U_{\perp}) \equiv \partial_r S(\exp(ir\sigma_{\gamma})U_{\perp})|_{r=0}, \quad (30)$$

where σ_{γ} , $1 \leq \gamma \leq N_c^2 - 1$ form a basis of $SU(N_c)$ algebra.. In particular,

$$D^{\gamma} U_{\perp} = i\sigma_{\gamma} U_{\perp}; \quad D^{\gamma} U_{\perp}^{\dagger} = -iU_{\perp}^{\dagger} \sigma_{\gamma}, \quad (31)$$

and derivatives of more complicated functions are obtained, combining these two rules with the usual rules of differentiation.

3.2 Initial conditions on the lattice

We now derive the lattice analogue of the continuum initial conditions in Eq. 11. We start from the lattice action in Eq. 28, obtain the lattice equations of motion in the four light cone regions and determine non-singular initial conditions by matching at $\tau = 0$ the coefficients of the most singular terms in the equations of motion.

On the lattice, the initial conditions are the constraints on the longitudinal gauge potential A^\pm and the transverse link matrices U_\perp at $\tau = 0$. The longitudinal gauge potentials are zero outside the light cone and satisfy the Schwinger gauge condition (Eq. 8) inside the light cone $x_\pm > 0$. Thus they can be written as in the continuum case (see Eq. 9) as

$$A^\pm = \pm x^\pm \theta(x^+) \theta(x^-) \alpha(\tau, x_t). \quad (32)$$

From our discussion in the last section, it is clear that the transverse link matrices are, for each nucleus, pure gauges before the collision. This fact is reflected by writing

$$U_\perp = \theta(-x^+) \theta(-x^-) I + \theta(x^+) \theta(x^-) U(\tau) + \theta(-x^+) \theta(x^-) U^{(1)} + \theta(x^+) \theta(-x^-) U^{(2)}, \quad (33)$$

where $U^{(1),(2)}$ are pure gauge.

The pure gauges are defined on the lattice as follows. To each lattice site j we assign two $SU(N_c)$ matrices $V_{1,j}$ and $V_{2,j}$. Each of these two defines a pure gauge lattice gauge configuration with the link variables

$$U_{j,\hat{n}}^{(q)} = V_{q,j} V_{q,j+\hat{n}}^\dagger, \quad (34)$$

where $q = 1, 2$ labels the two nuclei. As in the continuum, the gauge transformation matrices $V_{q,j}$ are determined by the color charge distribution $\rho_{q,j}$ of the nuclei, normally distributed with the standard deviation $g^4 \mu_L^2$ (compare with the continuum distribution in Eq. 4):

$$P[\rho_q] \propto \exp\left(-\frac{1}{2g^4 \mu_L^2} \sum_j \rho_{q,j}^2\right). \quad (35)$$

Parametrizing $V_{q,j}$ as $\exp(i\Lambda_j^q)$ with Hermitean traceless Λ_j^q , we then obtain Λ_j^q by solving the lattice Poisson equation

$$\Delta_L \Lambda_j^q \equiv \sum_n \left(\Lambda_{j+n}^q + \Lambda_{j-n}^q - 2\Lambda_j^q \right) = \rho_{q,j}. \quad (36)$$

It is easy to verify that the correct continuum solution (Eqs. 5 and 9) for the transverse fields A_\perp is recovered by taking the formal continuum limit of Eq. 33. Using the general representation of the gauge fields in Eqs. 32 and 33, we shall now derive the initial conditions for them at $\tau = 0$.

Initial conditions for $x^\pm > 0$: U_\perp

The equation of motion for U_\perp , contains, upon substitution of U_\perp from (33) and A^\pm from (32), two types of terms.

1. Terms regular at $x^\pm = 0$. All the terms containing less than two longitudinal derivatives belong to this category. The regularity of terms containing no longitudinal derivatives is clear. Terms in the action containing a single longitudinal derivative all involve the combination $A^- \partial_- + A^+ \partial_+$. Given the functional form (32) of A^\pm , these terms only give rise to regular contributions to the equation of motion. The double-derivative contributions $\Re\text{Tr}U_\perp^\dagger \partial_+ \partial_- U_\perp$ in the action give rise to terms in the equation of motion behaving as

$$\frac{1}{\tau} x^\pm \delta(x^\pm) \theta(x^\mp) \partial_\tau U,$$

which is regular if $\partial_\tau U$ vanishes rapidly enough as $\tau \rightarrow 0$. The terms regular at $x_\pm = 0$ provide no relation between U_\perp and $U^{(1),(2)}$.

2. The singular terms containing the product $\delta(x^+) \delta(x^-)$. These originate in the double-derivative contributions $\Re\text{Tr}U_\perp^\dagger \partial_+ \partial_- U_\perp$ in the action, when both derivative operators act on the step functions. Since the coefficient in front of $\delta(x^+) \delta(x^-)$ must vanish in order to satisfy the equation of motion, a matching relation between U and $U^{(1),(2)}$ is obtained.

We now compute the singular part of the U_\perp equation of motion. We note that

$$U_\perp (\partial_t^2 - \partial_z^2) U_\perp^\dagger = 2U_\perp (\partial_+ \partial_- U_\perp^\dagger) = 2(\partial_+ \partial_- U_\perp) U_\perp^\dagger$$

modulo a total derivative and utilize the identity $\theta(x)\delta(x) = \frac{1}{2}\delta(x)$ with the rules of Eq. 31. This gives, upon substitution of (Eq. 33) and retaining only the terms proportional to $\delta(x^+)\delta(x^-)$,

$$\text{Tr } \sigma_\gamma \left[(U^{(1)} + U^{(2)})(I + U^\dagger) - \text{h.c.} \right] = 0. \quad (37)$$

We therefore have obtained the result that $(U^{(1)} + U^{(2)})(I + U^\dagger)$ should have no anti-Hermitian traceless part. Note that this condition has the correct formal continuum limit: writing $U^{(1),(2)}$ as $\exp(ia_\perp\alpha_{1,2})$ and U as $\exp(ia_\perp\alpha_\perp)$, we have, for small a_\perp ,

$$\alpha_\perp = \alpha_1 + \alpha_2,$$

as required.

The above condition in Eq. (37) can easily be resolved in the SU(2) case, because the sum of any two 2×2 unitary matrices is a unitary matrix times a real number. Also, the anti-Hermitian part of an SU(2) matrix is traceless, while the Hermitian part is proportional to I. Therefore in this case Eq. 37 is equivalent to

$$(U^{(1)} + U^{(2)})(I + U^\dagger) = CI,$$

where C is a real number. Resolving this equation for U^\dagger and requiring that $U^\dagger U = I$, we obtain, after a simple calculation, that $C = \text{Tr}(U^{(1)} + U^{(2)})$ and hence

$$U = \frac{\text{Tr}(U^{(1)} + U^{(2)})}{U^{(1)\dagger} + U^{(2)\dagger}} - I = (U^{(1)} + U^{(2)})(U^{(1)\dagger} + U^{(2)\dagger})^{-1}. \quad (38)$$

For $N_c > 2$ the solution can be obtained by solving the $N_c^2 - 1$ equations (37) for the $N_c^2 - 1$ real numbers parametrizing U . The solution does not necessarily have the compact form (38). For simplicity, we leave the $N_c > 2$ case outside the scope of this paper.

Initial conditions for $x^\pm > 0$: A^\pm

We have seen that the matching conditions for the fields before and after the collision stem from the requirement that the singular terms in the equations of motion cancel

out. We now impose this requirement on the equation of motion for A_- . As before, the singularities arise only because longitudinal derivatives of step functions are taken.

Consider first the F_{+-}^2 term in the action. Since in this case we need two derivatives for a genuine singularity, we are only interested in the Abelian part of F_{+-}^2 , whose variation with respect to $A^{+, \gamma}$ gives

$$\frac{1}{N_c} \text{Tr} \sigma_\gamma \partial_+ (\partial_- A_+ - \partial_+ A_-),$$

whose most singular part is (using Eq. 32 and $x\delta'(x) = -\delta(x)$)

$$\alpha_\gamma \theta(x^-) \delta(x^+).$$

We now vary the \pm, \perp terms (Eq. 29) in the action (Eq. 28) with respect to $A_j^{\pm, \gamma}$ and select the contributions containing derivatives. The result is

$$-\frac{i}{2N_c} \sum_n \text{Tr} \sigma_\gamma \left[(\partial_+ U_{j-n, n}^\dagger) U_{j-n, n} - U_{j-n, n}^\dagger (\partial_+ U_{j-n, n}) - U_{j, n} (\partial_+ U_{j, n}^\dagger) + (\partial_+ U_{j, n}) U_{j, n}^\dagger \right],$$

the singular part of which is

$$\begin{aligned} & -\frac{i}{2N_c} \delta(x^+) \sum_n \text{Tr} \sigma_\gamma \left[\theta(x^-) (U^{(2)} - U^{(2)\dagger} + U^\dagger U^{(1)} - U^{(1)\dagger} U)_{j-n, n} \right. \\ & \quad \left. - \theta(x^-) (U^{(2)} - U^{(2)\dagger} + U^{(1)} U^\dagger - U U^{(1)\dagger})_{j, n} \right. \\ & \quad \left. + (U^{(2)\dagger} - U^{(2)})_{j-n, n} - (U^{(2)\dagger} - U^{(2)})_{j, n} \right]. \end{aligned} \quad (39)$$

Requiring that the coefficient in front of $\delta(x^+) \theta(x^-)$ vanish, we obtain

$$\alpha_\gamma = \frac{i}{2N_c} \sum_n \text{Tr} \sigma_\gamma \left[(U^{(2)} + U^{(1)} U^\dagger - \text{h.c.})_{j, n} - (U^{(2)} + U^\dagger U^{(1)} - \text{h.c.})_{j-n, n} \right].$$

This result can be cast in a more symmetric form, using the initial condition for U_\perp . Note that

$$U^{(2)} + U^{(1)} U^\dagger = \frac{1}{2} (U^{(1)} + U^{(2)}) (I + U^\dagger) + \frac{1}{2} (U^{(1)} - U^{(2)}) (U^\dagger - I).$$

Since the first term on the right-hand side has no anti-Hermitian traceless part, it follows that

$$\alpha_\gamma = \frac{i}{4N_c} \sum_n \text{Tr} \sigma_\gamma \left([(U^{(1)} - U^{(2)}) (U^\dagger - I) - \text{h.c.}]_{j, n} - [(U^\dagger - I) (U^{(1)} - U^{(2)}) - \text{h.c.}]_{j-n, n} \right). \quad (40)$$

It is easily seen that the above equation has the correct formal continuum limit. Writing again $U^{(1),(2)}$ as $\exp(ia_{\perp}\alpha_{1,2})$ and U as $\exp(ia_{\perp}\alpha_{\perp})$, we have, for small a_{\perp} ,

$$(U^{(1)} - U^{(2)})(U^{\dagger} - I) - \text{h.c.} \approx 2[\alpha_1, \alpha_2].$$

Hence, in the limit of smooth fields,

$$\alpha = i \sum_n [\alpha_1, \alpha_2]_n,$$

as required.

Finally, we require that the last line of Eq. 39 be cancelled by the term in the action coupling A^+ to the external source. This term then must have the form

$$\frac{i}{2N_c} \int dz dt \sum_j \delta(x^+) \text{Tr} A_j^+ \sum_n \left[(U^{(2)\dagger} - U^{(2)})_{j-n,n} - (U^{(2)\dagger} - U^{(2)})_{j,n} \right],$$

whose formal continuum limit is easily seen to be the correct one:

$$- \frac{1}{N_c} \int d^4x \delta(x^+) \text{Tr} A^+ \nabla \cdot A_{\perp}.$$

A completely analogous term should be included for A^- .

3.3 Hamiltonian formulation on the lattice

In the previous sub-sections, we wrote down the lattice action and lattice equations of motion for all regions of the light cone. Matching the singular terms on the light cone in section 3.2, we obtained the initial conditions for evolution in the forward light cone.

In section 2.3, we derived the continuum Hamiltonian for the forward light cone ($\tau > 0$) to be the Yang–Mills Hamiltonian in 2+1–dimensions in the gauge $A^{\tau} = 0$. The lattice Hamiltonian is obtained by performing a Legendre transform of Eq. 28 following the standard Kogut–Susskind procedure [42]. The analog of the Kogut–Susskind Hamiltonian here is

$$H_L = \frac{1}{2\tau} \sum_{l \equiv (j, \hat{n})} E_l^a E_l^a + \tau \sum_{\square} \left(1 - \frac{1}{2} \text{Tr} U_{\square} \right),$$

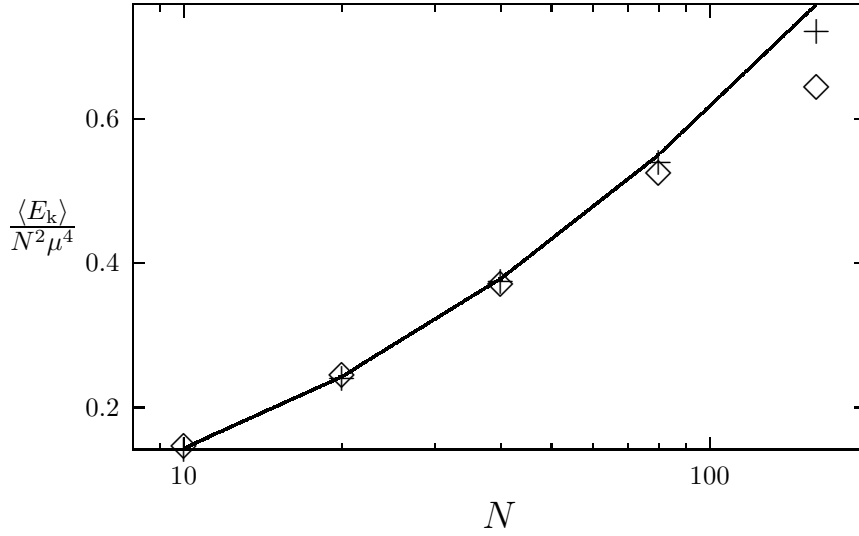


Figure 1: The lattice size dependence of the scalar kinetic energy density, expressed in units of μ^4 for $\mu = 0.0177$ (pluses) and $\mu = 0.035$ (diamonds). The solid line is the LPT prediction. The error bars are smaller than the plotting symbols.

$$+ \frac{1}{4\tau} \sum_{j, \hat{n}} \text{Tr} \left(\Phi_j - U_{j, \hat{n}} \Phi_{j+\hat{n}} U_{j, \hat{n}}^\dagger \right)^2 + \frac{\tau}{4} \sum_j \text{Tr} p_j^2, \quad (41)$$

where E_l are generators of right covariant derivatives on the group and $U_{j, \hat{n}}$ is a component of the usual $SU(2)$ matrices corresponding to a link from the site j in the direction \hat{n} . The first two terms correspond to the contributions to the Hamiltonian from the chromoelectric and chromomagnetic field strengths respectively. In the last equation, $\Phi \equiv \Phi^a \sigma^a$ is the adjoint scalar field with its conjugate momentum $p \equiv p^a \sigma^a$. Taking the continuum limit of the above Hamiltonian, one recovers the continuum Hamiltonian in Eq. 27.

Lattice equations of motion follow directly from H_L of Eq. 41. For any dynamical variable v with no explicit time dependence $\dot{v} = \{H_L, v\}$, where \dot{v} is the derivative with respect to τ , and $\{\}$ denote Poisson brackets. We take E_l , U_l , p_j , and Φ_j as

independent dynamical variables, whose only nonvanishing Poisson brackets are

$$\{p_i^a, \Phi_j^b\} = \delta_{ij}\delta_{ab}; \quad \{E_l^a, U_m\} = -i\delta_{lm}U_l\sigma^a; \quad \{E_l^a, E_m^b\} = 2\delta_{lm}\epsilon_{abc}E_l^c$$

(no summing of repeated indices). The equations of motion are consistent with a set of local constraints (Gauss' laws). These are

$$C_j^a \equiv \sum_{\hat{n}} \left[\frac{1}{2} E_{j,\hat{n}}^b \text{Tr} \left(\sigma^a U_{j,\hat{n}} \sigma^b U_{j,\hat{n}}^\dagger \right) - E_{j-\hat{n},\hat{n}}^a \right] - 2\epsilon_{abc} p_j^b \Phi_j^c = 0. \quad (42)$$

Explicitly, using the Poisson brackets above, the equations of motion for the four dynamical variables are as follows:

$$\dot{U}_m = \frac{-i}{\tau} U_m E_l, \quad (43)$$

$$\begin{aligned} \dot{E}_l &= \left\{ \tau \sum_{\square} \left(1 - \frac{1}{2} \text{Tr} U_{\square} \right), E_l \right\} \\ &\quad - \frac{i}{\tau} \left(\tilde{\Phi}_j \Phi_{j+\hat{n}} - \Phi_{j+\hat{n}} \tilde{\Phi}_j \right), \end{aligned} \quad (44)$$

$$\dot{\Phi}_j = \tau p_j \quad (45)$$

$$\dot{p}_j = \frac{1}{\tau} \left[\tilde{\Phi}_{j+\hat{n}}^\dagger + \tilde{\Phi}_{j-\hat{n}} - 2\Phi_j \right]. \quad (46)$$

Above, $\tilde{\Phi} = U_{j,\hat{n}} \Phi U_{j,\hat{n}}^\dagger$.

The results of section 3 can be summarized as follows. The four independent dynamical variables are E_l , U_{\perp} , p_j and Φ_j . Their evolution in τ after the nuclear collision is determined by Hamilton's equations above and their values at the initial time $\tau = 0$ are specified by the initial conditions derived explicitly in section 3.2. For easy reference, these are written compactly as follows:

$$\begin{aligned} U|_{\tau=0} &= (U_1 + U_2)(U_1^\dagger + U_2^\dagger)^{-1}; \quad E_l|_{\tau=0} = 0. \\ p_j|_{\tau=0} &= 2\alpha; \quad \Phi_j = 0, \end{aligned} \quad (47)$$

where U and α are given by Eq. 38 and Eq. 40 respectively. Note that the second set of conditions for Φ_j and p_j follows respectively from Eq. 25 and the definition of p_j —see the discussion after Eq. 24.

4 Interpreting lattice results for continuum physics

Before we turn to discussing in detail the numerical results from our lattice simulations, we should consider first the ramifications for the problem of nuclear collisions at very high energies. Specifically, we wish to know how one interprets in physical terms the results of our numerical simulations.

In section 2, we introduced a scale μ^2 , the color charge squared per unit area, and argued that new non-perturbative physics arises at momenta of order $k_t \sim \alpha_S \mu$. In the original work of McLerran and Venugopalan, only the valence quarks were taken to be sources of color charge which gave $\mu^2 \sim A^{1/3} \text{ fm}^{-2}$. Hence $\mu \gg \Lambda_{QCD}$ only for nuclei much larger than physical nuclei. However, if semi-hard gluons at x values greater than those of interest here ² are also included as sources of color charge as they should be, then μ^2 is significantly larger. Then μ^2 is defined as [24]

$$\mu^2 = \frac{A^{1/3}}{\pi r_0^2} \int_{x_0}^1 dx \left(\frac{1}{2N_c} q(x, Q^2) + \frac{N_c}{N_c^2 - 1} g(x, Q^2) \right), \quad (48)$$

where q, g stand for the *nucleon* quark and gluon structure functions at the resolution scale Q of the physical process of interest. Also, above $x_0 = Q/\sqrt{s}$. Using the HERA structure function data, Gyulassy and McLerran estimated that $\mu \leq 1 \text{ GeV}$ for LHC energies and $\mu \leq 0.5 \text{ GeV}$ at RHIC. Thus the regime where the classical Yang-Mills picture can be applied is rather limited. However, a window does exist and depending on what higher order calculations will tell us, this window may be larger or smaller than the naive classical estimates. Moreover, the insights gained from this self-consistent spacetime approach may still be very valuable in modelling heavy ion collisions which are not at the asymptotic energies where the approach becomes quantitative.

This work is not a quantitative study to be compared to experiment. Rather,

²Note that in this case, these correspond to those values of x corresponding to rapidities greater than the central rapidity in the nuclear collision.

our goal is a qualitative understanding of non-perturbative phenomena in the central region of a heavy ion collision. Towards this end, we need to

- relate lattice parameters to physical scales,
- define and compute quantities on the lattice that may be eventually compared to experiments with as little ambiguity as possible.

Let us first relate lattice units and physical units. Given A of a nucleus, we should match valence parton densities. To this end, we require the equality of cross-sectional areas. The relation between the linear size $L = Na$ of the lattice and the transverse radius R of the nucleus is then $L^2 = \pi R^2$. We ignore for the moment the difference in the lattice and continuum boundary conditions. For an $A = 200$ nucleus $R = 6.55$ fm translates into $L = 11.6$ fm. We can then express the lattice spacing $a = L/N$ in units of fermi.

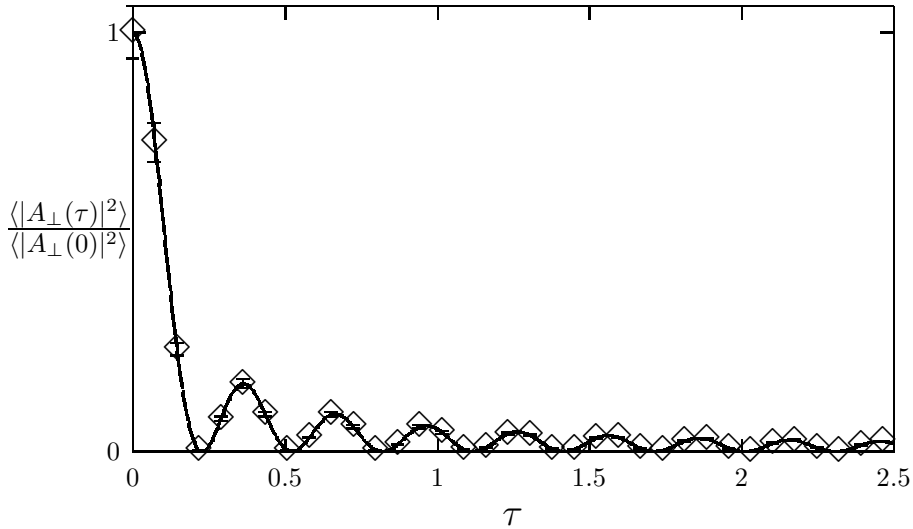


Figure 2: Normalized field intensity of a hard ($k_t = 2.16\text{GeV}$) mode vs proper time τ in units of fm (diamonds). Solid line is the LPT prediction.

Next, we determine the relation between the continuum μ and its lattice coun-

terpart. To do so, we use the Poisson equation (36) for the gauge transformation parameter Λ : $\Delta_L \Lambda = \rho_L$, and compare it to the continuum equation (7): $\Delta_\perp \Lambda = \rho_c$. For $a \rightarrow 0$ the lattice Laplacian Δ_L approaches $a^2 \Delta$, hence we must have $\rho_L = \rho_c a^2$. Also, as $a \rightarrow 0$, the lattice and continuum distributions of the color charge should become identical. Keeping in mind that $a^2 \Sigma = \int dx_\perp^2$ for small a , we obtain $\mu_L = a \mu_c$. In the effective theory on the lattice the coupling is $g^2 \mu_L L$ [43]. In this qualitative work, for simplicity, we choose $g = 1$. Then $\mu_L = 0.1$, for instance, for an $A = 200$ nucleus corresponds to

$$\mu_c = \frac{0.1}{a} \rightarrow 0.1 \frac{N}{L} \sim 0.28 \text{ GeV for } N=160. \quad (49)$$

For a physical scale of say $\mu = 0.6$ GeV, and the number of sites $N = 160$, we should pick $\mu_L \sim 0.21$. To compare lattice momenta to momenta in physical units, note that $k_t = 2\pi n/L$, where $-(N-1)/2 \leq n \leq (N-1)/2$. Then, for $L = 11.6$ fm, $k_t \sim 1$ GeV for $n \sim 9-10$. For $\mu_c = 1$ GeV or equivalently, $\mu_L = 0.36$, one may expect perturbation theory to be reliable for $n \geq 10$. One can in principle estimate the value of n where strong coupling effects become significant.

There still remains the question of how to relate lattice time τ_{latt} to the time in physical units, τ_{phys} . This can be obtained by comparing the continuum and lattice Hamiltonians at small a , [30]

$$\tau_{\text{phys}} = a \tau_{\text{lattice}}.$$

Recall that $a = L/N$ fm. For $L = 11.6$ and $N = 160$, $a = 0.07$ fm.

Now that we have straightened out the relation of lattice units to physical units, we must consider what can be measured on the lattice. Interesting quantities would be those for which our simulations would predict non-perturbative corrections to “empirical” quantities which can be computed in perturbative QCD at large momenta. A quantity one may consider is the cross section for gluon mini-jet production. At large transverse momenta, Gyulassy and McLerran [24] have shown that the clas-

sical Yang–Mills formula in Eq. 21 is at small x (approximately) the same as the perturbative QCD prediction [13] for the process $AA \rightarrow g$

$$\frac{d\sigma}{dyd^2k_t} = K_N \frac{\alpha_S N_c}{\pi^2 k_t^2} \int d^2q_t \frac{f(x_1, q_t^2) f(x_2, (\vec{k}_t - \vec{q}_t)^2)}{q_t^2 (\vec{k}_t - \vec{q}_t)^2}, \quad (50)$$

where

$$f(x, Q^2) = \frac{dxG(x, Q^2)}{d \log Q^2}, \quad (51)$$

and $x_1 \approx x_2 = k_t/\sqrt{s}$. The two formulae are equivalent if we divide the above formula by πR^2 , approximate the integral above by factoring out f above at the scale k_t^2 and taking the normalization factor $K_N \approx 5$. At large transverse momenta therefore, we can relate the field intensity measured on the lattice $|A_{k_t}|^2$ for the appropriate values of μ to the cross section for $AA \rightarrow g$. The lattice perturbation theory expression (which matches the prediction of the full theory at large momenta) is given by Eq. 69 of appendix B.

However, at smaller transverse momenta, there is no simple relation between the field intensity and the classical gluon distribution function (and thereby the cross section by the above arguments). This is because the dispersion relation for soft gluons is not that for free gluons—the interpretation of the field intensity as the gluon distribution is then clearly not right. We have to look for more general gauge invariant quantities which, conversely, in the limit of large k_t , will give us the $AA \rightarrow g$ cross section.

Some of the quantities we can compute on the lattice in strong coupling and in principle compare to experiment are quantities related to various components of the energy–momentum tensor. In an interesting recent paper, Testa has shown [53] that a class of semi–inclusive observables (such as, for example, the energy flux through a surface corresponding to the resolution of a detector) can be related to various components of the energy–momentum tensor. Our eventual goal is to compute in the classical effective theory, non–perturbative corrections to the energy–energy correlators measured in jet physics [54].

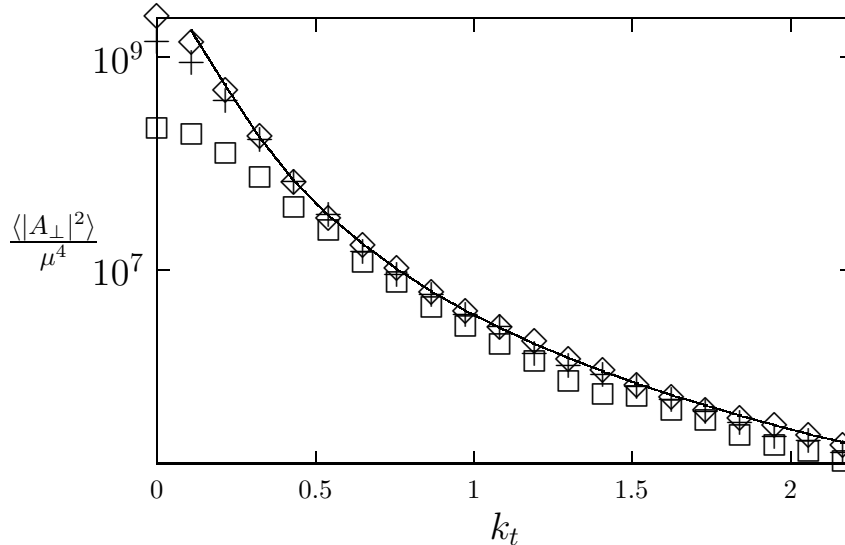


Figure 3: Field intensity over μ^4 as a function of k_t for $\mu = 200\text{MeV}$ (squares), $\mu = 100\text{MeV}$ (pluses), and $\mu = 50\text{MeV}$ (diamonds). Solid line is the LPT prediction. The field intensity is in arbitrary units and k_t is in GeV.

In this work, we measure a variety of observables. On the one hand, extensive quantities like the energy, with well defined local gauge-invariant densities, provide useful information on the system and are easily measurable. On the other hand, in an experiment one usually deals with gluon fields with definite momenta. Such fields are not easy to define outside perturbation theory. In order to study momentum distributions of gluons, we introduce two types of quantities.

First, we define the gauge field on every link of the lattice as the imaginary part of the link matrix. Note that we work in the $A_\tau = 0$ gauge and fix the Coulomb gauge in the transverse plane for $\tau = 0$. Hence there is no gauge freedom left in our definition of the gauge field. The same applies for the scalar field. In the following, we will study the momentum dependence of these gauge-fixed objects.

Secondly, we consider a gauge-invariant estimate of the gluon energy in terms of equal time energy–energy correlators. We make use of the fact that each of the kinetic

and potential terms in (41) are squared quantities such as E^2 and B^2 . Consider, for instance, the connected correlator in the Abelian case

$$C_m(x_t) = \langle B^2(x_t)B^2(0) \rangle_\rho - \langle B^2(x_t) \rangle_\rho \langle B^2(0) \rangle_\rho. \quad (52)$$

If the distribution of B were normal, $P[B] \propto \exp(h[B])$, with a translation-invariant bilinear functional h , $C_m(x_t)$ would factorize:

$$C_m(x_t) = 2\langle B(x_t)B(0) \rangle_\rho^2 \geq 0. \quad (53)$$

Following the analogy with this special Abelian case, we *define* the magnetic energy of the momentum mode k_t in the non-Abelian theory as

$$E_m(k_t) \equiv \frac{1}{2\sqrt{N}} \sum_{\mathbf{x}_t} e^{i\mathbf{k}_t \cdot \mathbf{x}_t} \sqrt{\frac{1}{2}C(x_t)}. \quad (54)$$

The analog of (54) can be defined for each of the six potential and kinetic terms (counting the chromo-electric and the scalar potential terms separately for each lattice direction) in (41). The total energy distribution in momentum space is then defined as the sum of these six contributions.

Before we end this section, we should comment on the continuum limit in this approach. The theory contains dimensionful quantities, μ and L , which may be related to physical observables. One approaches the continuum limit by keeping μL fixed and taking μ in lattice units to zero. Comparing dimensionless ratios of physical observables to their lattice counterparts would then allow one to extract the continuum value of μL . In this theory, the field amplitudes squared fall off as $1/k^4$ as opposed to a thermal field theory where the field amplitudes squared fall off as $1/k^2$. It is therefore more likely that a wider range of physical observables will have a well defined continuum limit than in the thermal case. Whether this is indeed the case requires a careful study of physical (gauge invariant) observables by taking the continuum limit of their lattice counterparts in the manner prescribed above. We plan to continue this study in a future work.

Finally, we mention here for future reference a proper-time lattice computation of an interesting gauge-invariant quantity that can be directly related to experiment, namely, the Poynting vector. The Poynting vector describes the energy flux out of the nuclear surface. It, and other components of the energy-momentum tensor, can be defined on the lattice [52]. Computing the Poynting vector however requires a more careful choice of boundary conditions than the periodic boundary conditions described in this work. This too will be left to a future study.

5 Real time lattice computation of gluon production: results

We now turn to numerical results from our simulations. These were performed for a variety of lattice sizes $L= 20-160$ and the color charge density $\mu = 0.015-0.2$ in units of the lattice spacing a . To convert lattice results to physical units, we take $L^2 \approx \pi R^2$ for $A=200$ nuclei. This then also determines μ for a fixed lattice size. The relation of lattice time to continuum time is given by the relation $\tau_C = a \cdot \tau_L$ [30]. In Fig. 1, we plot the Gaussian averaged initial kinetic energy $\langle E_k \rangle$ on the lattice as a function of the lattice size L and compare it with the lattice perturbation theory expression (Eq. 73 in appendix B) for different values $\mu_L = 0.0177, 0.035$ of the color charge density. For small values of L , there is very good agreement between the two but for the largest value $L = 160$, they begin to deviate. Since the strong coupling parameter on the lattice is $\propto g^2 \mu_L L$, for $g^2 \mu_L L \gg 1$ we can expect to see deviations from lattice perturbation theory.

In Fig. 2, we plot the ratio of the field intensity of a particular mode of the transverse gauge field as a function of proper time τ normalized to its value at $\tau = 0$. The diamonds are results from a lattice simulation with $L = 160$ and $\mu_L = 0.0177$ and the mode considered is $(k_x, k_y) = (\pi/4, 0)$. Note that $k_{x,y} = 2\pi n_{x,y}/L$ and for this

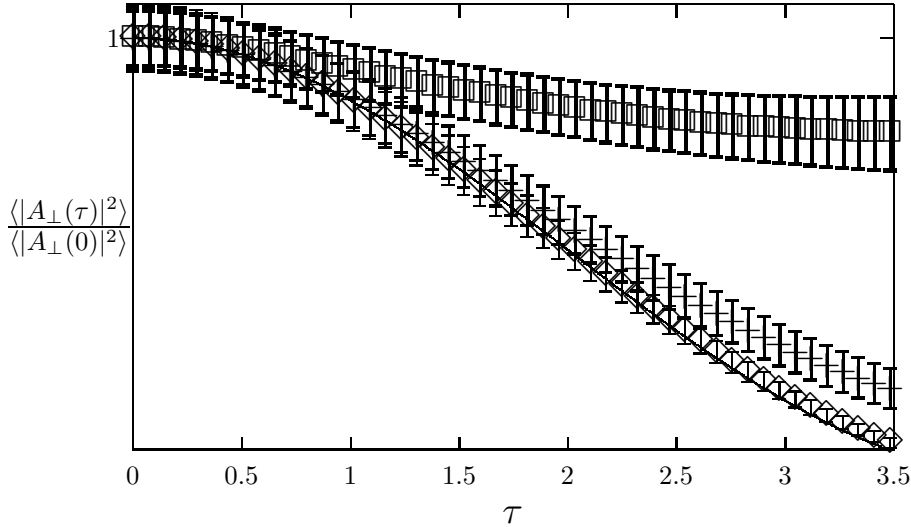


Figure 4: Normalized field intensity of a soft ($k_t = 108\text{MeV}$) mode vs proper time τ (in units of fm) for $\mu = 200\text{MeV}$ (squares), $\mu = 100\text{MeV}$ (pluses), and $\mu = 50\text{MeV}$ (diamonds). Solid line, nearly coinciding with the $\mu = 50\text{MeV}$ curve, is the LPTth prediction.

case, $n_x = 20, n_y = 0$. The solid line in the figure is the square of the Bessel function $J_0(\omega\tau)$ where $\omega = \sqrt{2(2 - \cos(k_x) - \cos(k_y))}$. Since the τ -direction in our simulation is continuous, the time dependence of the high transverse momentum perturbative modes should agree with the continuum perturbative result which predicts a time dependence proportional to $J_0^2(\omega\tau)$ for the field intensity of the transverse gauge fields. The continuum dispersion relation $\omega = |k_{\perp}|$ is however modified into the lattice dispersion relation shown above. We see from the figure that the anticipated agreement between the lattice results and perturbation theory is quite good.

In Fig. 3, the field intensity of the transverse gauge field normalized by μ^4 at $\tau = 0$ is plotted as a function of the transverse momentum in physical units. The lattice results for the different values of μ described in the caption are compared to lattice perturbation theory result—Eq. 69 in appendix B—for the field intensity. The

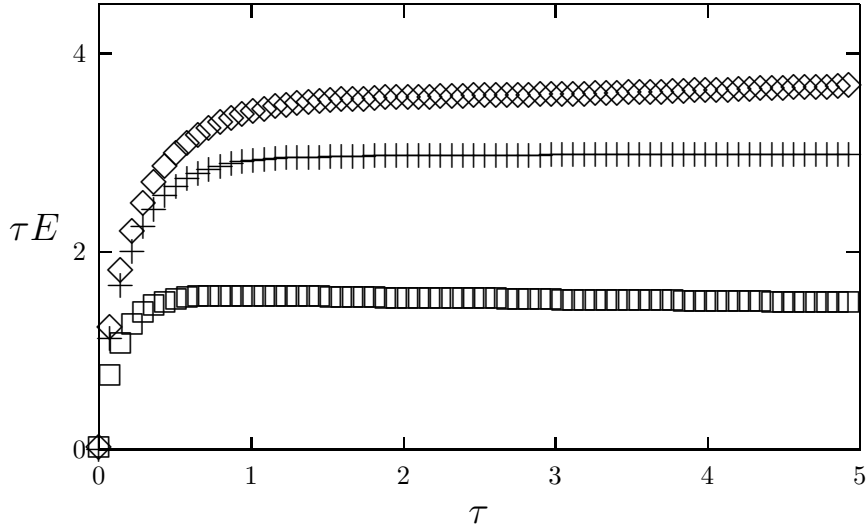


Figure 5: Time history of the energy density in units of μ^4 for $\mu = 200\text{MeV}$ (squares), $\mu = 100\text{MeV}$ (pluses), and $\mu = 50\text{MeV}$ (diamonds). Error bars are smaller than the plotting symbols. Proper time τ is in fm.

LPT_h result (which would be the mini-jet distribution in the continuum) agrees very well with the lattice result for small μ upto very small values of k_t . However, strong coupling effects grow with increasing μ (the lattice size L is fixed here) and we see deviations from the perturbative predictions at larger values of k_t . This trend is enhanced further at larger values of μ than those shown here. The non-perturbative effects due to the non-linearities in the Yang-Mills equations seem to temper the $1/k_t^4$ behaviour predicted by perturbation theory. Whether this reflects the presence of a mass in the theory needs further investigation.

In Fig. 4, we plot the same quantity as in Fig. 2, but now for three different values of μ and for the first non-zero momentum mode $(k_x, k_y) = (1, 0)$. The lattice size $L = 160$ is the same as previously. For the smallest value of $\mu = 0.0177$, there is again an agreement with the Bessel behaviour predicted by perturbation theory. However at the larger values of $\mu_L = 0.035, 0.07$, one sees significant deviations away

from the Bessel behaviour. Indeed, the modes seem to saturate at larger values of τ . At face value this is unexpected because one expects that as the systems cools at late times, even the small k_{\perp} modes should eventually die out. It may be that we have to wait for times much longer than those studied to see this. That would indeed be very interesting because these times would be much greater than the natural time scale $\tau \sim 1/g^2\mu$ at which we expect non-linearities to dissipate (see the discussion of Fig. 5 below).

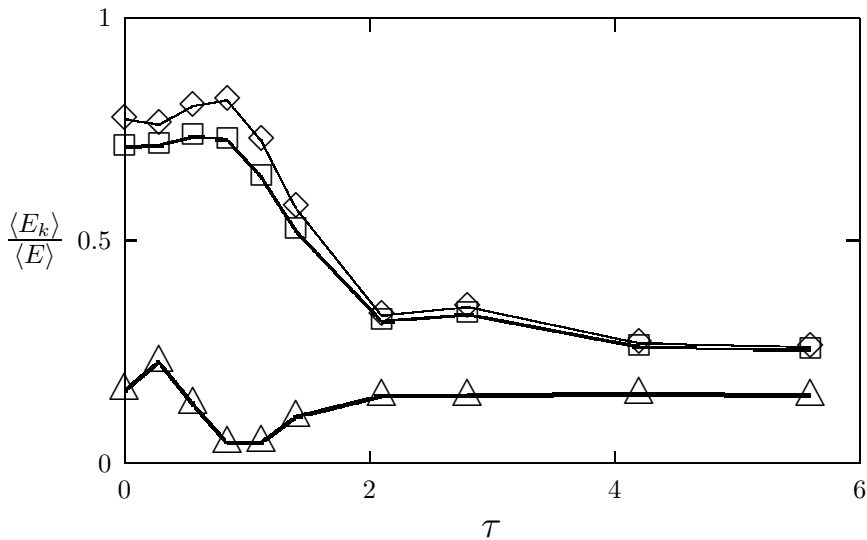


Figure 6: Energy per mode k normalized to the total energy as a function of proper time in fermis. From top to bottom, the curves correspond to modes $k = 0, 108$ and 432 MeV respectively. As in the previous figure, $\mu = 0.41$ GeV.

A straightforward explanation for this behaviour is that it is some kind of gauge artifact. This is because even though the fields satisfy the Coulomb gauge condition at $\tau = 0$, they no longer do so at later times. Thus one may need to fix Coulomb gauge at each “measured” time to properly interpret what we have called as field intensities as such. Large modes may be unaffected by the gauge fixing but small modes will

be affected. The simplest test of this explanation is to study the correlators of gauge invariant quantities at late times. If they display the same “saturation” then the effect cannot be dismissed as a gauge artifact. We will return to this point a little later.

Before we do that, we would like to discuss the time dependence of the energy density, shown in Fig. 5 for different values of μ . At late times, from general considerations we expect that $E \propto 1/\tau$ and that is what we see. Indeed, we can see qualitatively that the time at which this behaviour is seen is roughly $\propto \frac{1}{g^2\mu}$.

Thus, even though we clearly see non-perturbative behaviour at low k_t , the apparent saturation of these modes at large times has no impact on the behaviour of the energy density at late times. As μ is decreased, the magnitudes of the energy density appear to converge to a fixed value. This behavior of the energy has a purely kinematic reason: for any fixed finite rapidity the proper time τ asymptotically approaches the real time t , with respect to which the energy is conserved. LPT_h also predicts this behavior.

We now describe preliminary estimates of the energy distribution, obtained from energy-energy correlators, as described in Section 4. The computation was performed for an 80×80 lattice and for $\mu = 0.41$ GeV. With the small data sample available (50 independent configurations for the values of proper time τ considered), we found that the correlation functions $C(x_t)$ are consistent with 0 at distances $|x_t| \geq 12$ in lattice units. We therefore approximated $C(x_t)$ as 0 for $|x_t| \geq 12$. While the quality of our data at this point does not permit a quantitative description of the gluon distribution, the data do help us address the question as to whether the unusual behavior of the soft modes, as shown in Figure 4, has observable consequences.

In Fig. 6, we plot the time dependence of the ratio of the energy of the k th mode to the total energy of the system (measured directly). The ratio, for the momenta considered (0, 108 and 432) MeV, goes to a constant at late times. Since Fig. 5 clearly shows that the energy dies off as $1/\tau$, our result suggests that at late times the energy

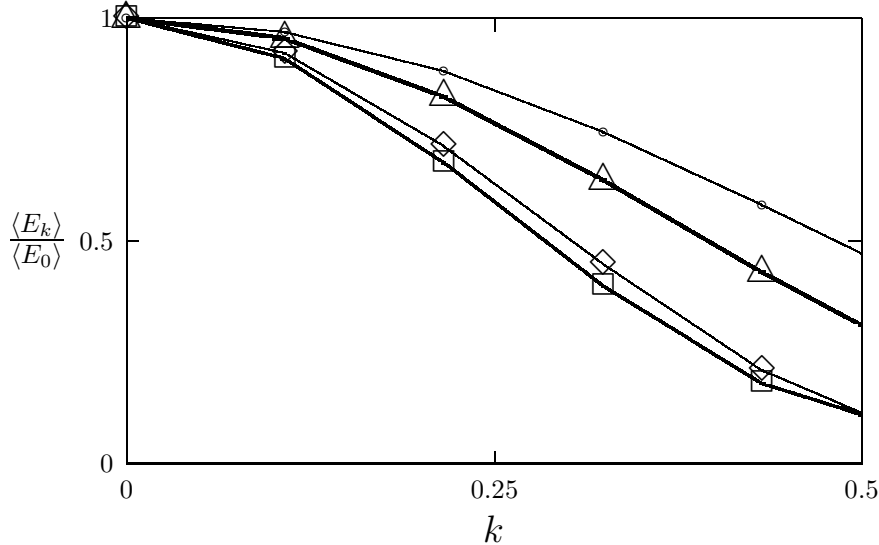


Figure 7: Energy per mode k normalized to energy of zeroth mode as a function of k in GeV units. From bottom to top, the curves correspond to proper times of $\tau = 0, 1.4, 2.8, 5.6$ fermis. Here $\mu = 0.41$ GeV.

of the low k_t modes must die off as $1/\tau$ too. We therefore have an indication that the apparent saturation of the field intensities in Fig. 4 is not meaningful and is a gauge artifact.

In Figure 7, we plot the total energy per mode normalized to the energy of the zeroth mode as a function of k for the proper times (from bottom to top) $\tau = 0, 1.4, 2.8, 5.6$ fm. Interestingly, the ratio plotted gets flatter at larger values of τ . We interpret this to mean that the share of the energy in the lower- k_t modes decreases at late times. This is another indication of a benign behavior of soft modes at late times, contrary to what is suggested by Figure 4.

6 Summary and outlook

In this paper, we have performed a non-perturbative study of the production and space-time evolution of gluon mini-jets in the central region of nuclear collisions at

very high energies. This program was proposed in Ref. [32] and a brief discussion of our results can be found in Ref. [55].

Our work is based on a classical effective field theory description of the small x modes in nuclei at very high energies. This effective theory contains a scale μ which is proportional to the large gluon density at small x . The large gluon density ensures that even if the coupling is weak, the fields may be highly non-perturbative. Since the approach is classical, it is possible to study the real time evolution of these non-perturbative modes in a nuclear collision. The approach has the attractive feature that it may eventually provide a self-consistent picture of high energy nuclear collisions both before and after the nuclei collide.

At large transverse momenta, $k_t \gg \alpha_S \mu$, the predictions of the effective theory for gluon production should agree with perturbative mini-jet calculations. As discussed in Section 5, our lattice results agree with the lattice perturbation theory analogue of the continuum mini-jet predictions. At smaller transverse momenta, (in particular for large μ) we see significant deviations from perturbation theory. We also notice that the field intensities, $|A(k_t, \tau)|^2$, of the small k_t modes do not die off at the late times studied but appear to saturate.

It is difficult to interpret the behaviour of the small k_t modes since they are “off-shell”: their dispersion relation $\omega(k_t)$ is non-trivial. Unlike the large momentum limit, the field intensities for the small k_t modes does not have the simple interpretation of being the number distribution of produced gluons. As discussed in the previous section it is therefore important to look at gauge invariant quantities which can be interpreted straightforwardly. In the previous section we discussed a number of gauge invariant equal time spatial correlators. These correspond to correlators of components of the energy-momentum tensor. In particular, we suggested a gauge invariant estimate of the energy distribution on the lattice as a function of time. In principle, we should be able to compute the range of energy-energy correlators measured in high energy collisions (see Basham et al. [54] and references therein). A more

extensive discussion of these correlators will be presented at a later date [47].

An important issue not addressed in this work is that of equilibration—do the gluons produced equilibrate? We saw in Fig. 5 that the energy density shows the expected behaviour after times $\propto 1/g^2\mu$. This however is no proof of thermalization. In the classical approach, clearly the high k_t modes are not “thermal”. Whether this is the case for the softer modes needs to be studied further. It would be interesting to relate this approach to that of Müller and collaborators [48, 49, 50].

We would like to stress that this work is not a quantitative study of gluon production in heavy ion collisions but a qualitative study of non-perturbative effects that may be important in the central region of these collisions. Changes that can be made in future to bring our results closer to experiment include a) changing the gauge group to SU(3), b) relaxing the boost invariance assumption, and c) modifying the boundary conditions. Regarding the last point, we have used periodic boundary conditions. Modifying these would, for instance, be useful in computing the Poynting flux through the nuclear surface.

Though our choice of gauge $A^\tau = 0$ is convenient from the point of view of a lattice simulation, results in this gauge do not lend themselves easily to a diagrammatic interpretation. In this regard it might be useful also to consider a similar computation in Coulomb gauge where this is the case [51]. Results of such computation will be presented at a later date.

Acknowledgments

We would like to thank the Universidade do Algarve (RV) and the Niels Bohr Institute (AK) for their kind hospitality. We would also like to thank M. Gyulassy, Yuri Kovchegov, Alex Kovner, B. Müller, Rob Pisarski, J. Randrup, Dirk Rischke and X.-N. Wang for useful comments and discussions. We would like to thank Larry McLerran for his critical input and encouragement during the course of this work.

RV's work is supported by the Danish Research Council and the Niels Bohr Institute. Both AK and RV acknowledge support provided by the Portuguese Fundação para a Ciência e a Tecnologia, grants CERN/S/FAE/1111/96 and CERN/P/FAE/1177/97.

Appendix A: Numerical method

In integrating equations of motion of a classical gauge theory it is important to ensure that the redundant gauge degrees of freedom do not become observable through numerical errors. Hence the integration scheme must respect the Gauss constraints of the theory. To this end, the algorithm of choice for the problem at hand is the leapfrog algorithm [46]. This integration scheme requires that the Hamiltonian be a sum of gauge-invariant kinetic K (dependent on fields only) and potential V (dependent on conjugate momenta only) terms, and under this condition, has the advantage of respecting the Gauss constraints exactly [45]. Our lattice Hamiltonian (41) obviously has the necessary $K + V$ form, thus the leapfrog algorithm is applicable.

The light-cone Hamiltonian (41) depends explicitly on the proper time τ . For this reason, the standard leapfrog scheme, designed for time-independent Hamiltonian functions, requires some minor adaptation in the present case. In order to explain the suitable version of the algorithm, we collectively denote the E , p momentum³ variables by P and the U , Φ field variables by Q , respectively. The K and V terms in the Hamiltonian then have the form $K(P, \tau)$ and $V(Q, \tau)$. In the following, the argument τ of K or V is thought of as a *fixed parameter*. With this notation, the leapfrog step of size Δ , propagating the system in proper time from τ to $\tau + \Delta$, has the following form.

1. Integrate the equations $\dot{Q} = \{K(P, \tau), Q\}$ between τ and $\tau + \Delta/2$.

³Strictly speaking, E variables are not conjugate momenta. Indeed, their Poisson brackets with each other do not necessarily vanish. However, the scheme as presented only requires that $\{K, E\} = 0$, and E need not be momentum variables.

2. Integrate the equations $\dot{P} = \{V(Q, \tau + \Delta/2), P\}$ between τ and $\tau + \Delta$.
3. Integrate the equations $\dot{Q} = \{K(P, \tau + \Delta), Q\}$ between $\tau + \Delta/2$ and $\tau + \Delta$.

Here the integration of the equations of motion is assumed to be performed exactly at every substep. It can be readily seen that the step as described is exactly reversible, *i.e.*, beginning with the final values of P, Q and performing the step with Δ replaced by $(-\Delta)$, one arrives at the initial P, Q . This property of the leapfrog algorithm, evident for a time-independent Hamiltonian, is preserved here by suitably choosing the explicit proper-time argument of K and V at each substep. The time reversibility guarantees that the integration error, obviously of the order no lower than Δ^2 , is in fact $\mathcal{O}(\Delta^3)$.

In order to impose the initial conditions for the proper-time Hamiltonian evolution, we first need to solve the lattice Poisson equation (36). We do so using the over-relaxation method [56]. The consistency of Eq. 36 requires that the zero-momentum component of the color charge density ρ vanish. We therefore first generate the color charge distribution as a normal deviate (35), then subtract from every $\rho_{q,j}$ the spatial average $\sum_j \rho_{q,j}/N$.

We fix the Coulomb gauge on initial configurations (see also the discussion in section 2.2). The lattice Coulomb gauge reads

$$\text{Tr} \left[\left\{ \sum_n \left(U'_{j,\hat{n}} - U'_{j,\hat{n}}{}^\dagger \right) - \sum_n \left(U'_{j-n,\hat{n}} - U'_{j-n,\hat{n}}{}^\dagger \right) \right\} \sigma^a \right] = 0, \quad (55)$$

where $U'_{j,\hat{n}}$ is the link matrix which satisfies the Coulomb gauge condition (55). We use the standard overrelaxation method [57] for gauge fixing.

Appendix B: Lattice perturbation theory

At large transverse momenta, a test of our lattice results is that they agree with those of lattice perturbation theory. Here we present a derivation of classical gluon

production in lattice perturbation theory. In the continuum limit, we will show that our result agrees with Eq. (27) of Ref. [23]. We also obtain an expression for the initial kinetic energy on the lattice. We will later compare these analytical expressions to the full lattice results at large transverse momenta.

We restrict our discussion to the gauge group $SU(2)$ and consider the initial condition (38) for the link matrix U

$$U = (U^{(1)} + U^{(2)})(U^{(1)\dagger} + U^{(2)\dagger})^{-1}.$$

Here the labels of the nuclei are written as superscripts. Now recall that since $U_{j,n}^{1,2}$ are pure gauges, they can be written as (see Eq. 34)

$$U_{j,n}^{(i)} = V_j^{(i)} V_{j+n}^{(i)\dagger},$$

where $V_j^{(i)} = \exp(i\Lambda_j^{(i)})$ and $i = 1, 2$. Hence,

$$U_{j,n}^{(i)} = 1 + i \left(\Lambda_j^{(i)} - \Lambda_{j+n}^{(i)} \right) + \left(\Lambda_j^{(i)} \Lambda_{j+n}^{(i)} - \frac{1}{2} \left[(\Lambda_j^{(i)})^2 + (\Lambda_{j+n}^{(i)})^2 \right] \right) + O(\Lambda^3). \quad (56)$$

The pure gauge solution of the Yang–Mills equations for a single nucleus dictates that $\nabla_{\perp}^2 \Lambda^{(i)} = \rho^{(i)}$ (see also Eq. 6). Therefore $\Lambda \sim O(\mu)$ and we have kept terms in the expansion above up to $O(\mu^2)$. Then substituting Eq. 56 in the expression for U , we obtain

$$U_{j,n} = I + iL_{j,n} + \frac{1}{2} \left(Q_{j,n} - Q_{j,n}^{\dagger} - L_{j,n}^2 \right) + O(\mu^3), \quad (57)$$

where I is the $SU(2)$ identity matrix,

$$L_{j,n} = \sum_{i=1}^2 \left(\Lambda_j^{(i)} - \Lambda_{j+n}^{(i)} \right) \equiv \alpha_{j,\hat{n}}^{(1)} + \alpha_{j,\hat{n}}^{(2)}, \quad (58)$$

and

$$Q_{j,n} = \sum_{i=1}^2 \left[\Lambda_j^{(i)} \Lambda_{j+n}^{(i)} - \frac{1}{2} \left((\Lambda_j^{(i)})^2 + (\Lambda_{j+n}^{(i)})^2 \right) \right]. \quad (59)$$

We work in the $A_\tau = 0$ gauge, supplemented by the Coulomb gauge condition (55) at $\tau = 0$. The Coulomb gauge-transformed link matrix U' is related to the original link U as

$$U_{j,n}' = W_j U_{j,n} W_{j+n}^\dagger.$$

This is analogous to the transformation carried out in the continuum perturbation theory derivation discussed in section 2.2. For $\mu = 0$ the Coulomb gauge is satisfied by the trivial configuration $U = I$, Hence the gauge transformation W_j can be expanded in powers of small μ :

$$W_j = \exp\left(I + i\mu\xi_j + i\mu^2\eta_j + \mathcal{O}(\mu^3)\right).$$

We now need to determine ξ and η from the Coulomb gauge condition (55). Writing out U' to order μ^2 , we obtain

$$\begin{aligned} U_{j,n}' &= I + i\mu(\xi_j - \xi_{j+n} + L_{j,n}) + \mu^2\left(i(\eta_j - \eta_{j+n}) - \frac{1}{2}(\xi_j^2 + \xi_{j+n}^2)\right. \\ &\quad \left.+ \xi_j\xi_{j+n} + (L_{j,n}\xi_{j+n} - \xi_j L_{j,n}) + \frac{1}{2}(Q_{j,n} - Q_{j,n}^\dagger - L_{j,n}^2)\right). \end{aligned} \quad (60)$$

To lowest order, the Coulomb gauge condition (60) implies that

$$\xi_j - \xi_{j+n} = -L_{j,n} \longrightarrow \xi_j = -\left(\Lambda_j^{(1)} + \Lambda_j^{(2)}\right). \quad (61)$$

Now consider the Coulomb gauge condition to order μ^2 . We need to determine η_j to obtain W_j to that order. After some algebra, one can show that

$$\eta_j = \frac{1}{2i} \frac{1}{\Delta} \left\{ [\Lambda_j^{(1)}, \Lambda_{j-n}^{(2)} + \Lambda_{j+n}^{(2)}] + (1) \leftrightarrow (2) \right\}. \quad (62)$$

Above, Δ is the usual lattice Laplacian

$$\Delta(l) = 2 \sum_{n=1,2} (1 - \cos(l_n)),$$

and $l_n = k_n \cdot a$. Having computed ξ and η using the Coulomb gauge fixing condition, we are now in a position to compute α' —the lattice analog of the field ϵ^i in section 2.

We have

$$2i\alpha'_{j,n} = U_{j,n'} - U_{j,n}{}^{\dagger} \equiv 2i(\eta_j - \eta_{j+n}) - \left([\Lambda_j^{(1)}, \Lambda_{j+n}^{(2)}] + (1) \leftrightarrow (2)\right) + \mathcal{O}(\mu^3). \quad (63)$$

To determine the field intensity we need to compute the lattice Fourier transform of the above expression. Using the Fourier transform of Λ ,

$$\Lambda_j^{(1),b} = \frac{1}{N^2} \sum_{p=-(N-1)/2}^{(N-1)/2} \exp(2\pi i \vec{p} \cdot \vec{x}_j/L) \tilde{\Lambda}_l^{(1),b}, \quad (64)$$

after quite some algebra, we obtain the result that

$$\begin{aligned} \alpha'_{l,n}{}^a &= \frac{\epsilon^{abc}}{N^2} \left[\sum_{l'} \left\{ \left(\frac{1 - e^{il_n}}{\Delta(l)} \right) \left(\sum_{n'} (-) 2 \sin\left(\frac{l_{n'}}{2}\right) \sin\left(\frac{l_{n'}}{2} - l'_{n'}\right) \right) \right. \right. \\ &\quad \left. \left. - i e^{il_n/2} \sin\left(\frac{l_n}{2} - l'_n\right) \right\} \tilde{\Lambda}_{l'}^{(1),b} \tilde{\Lambda}_{l-l'}^{(2),c} \right]. \end{aligned} \quad (65)$$

It is useful to compare this result to the corresponding continuum expression. Here and in the following the continuum result is obtained by setting $\alpha'_l \rightarrow \alpha'_k a/g$, $l_n \rightarrow k_i a$ and $\sum_{l'} \rightarrow L^2 \int \frac{d^2 k'}{(2\pi)^2}$ and letting $a \rightarrow 0$. In the case of Eq. 65 this prescription gives

$$\alpha'_{k,n}{}^a = \epsilon^{abc} \int \frac{d^2 k'}{(2\pi)^2} \left(\frac{k_n k_{n'}}{k^2} - \delta_{ij} \right) \tilde{\Lambda}_{k'}^{(1),b} i(k_{n'} - k'_{n'}) \tilde{\Lambda}_{k-k'}^{(2),c}, \quad (66)$$

This result is identical to the Fourier transform of Eq. (27) in Kovner, McLerran and Weigert [23].

We can now compute the field intensity directly. It is defined as

$$|\alpha'_l|^2 = \sum_n \langle \alpha'_{l,n}{}^a \alpha'_{-l,n}{}^a \rangle_\rho, \quad (67)$$

where $\langle \dots \rangle_\rho$ denotes the Gaussian averaging over the sources. On the lattice, the continuum condition $\nabla_\perp^2 \Lambda^{(i)} = \rho^{(i)}$ translates into

$$\tilde{\Lambda}_l^{(i)} = -\mu L \frac{\eta_l^{(i)}}{\Delta(l)}, \quad (68)$$

where $\eta_l = \tilde{\rho}_l a^2 / \mu L$. Hence $\langle \eta_l \rangle_\rho = 0$ and $\langle \eta_l \eta_{l'} \rangle_\rho = \delta_{l,-l'}$. Substituting Eq. 65 in Eq. 67 and performing the averaging over ρ 's, we obtain finally the following expression for the field intensity

$$|\alpha'_l|^2 = \frac{3\mu^4}{2\Delta(l)} \sum_{l'}' \frac{\Delta(2l' - l)\Delta(l) - [\Delta(l' - l) - \Delta(l')]^2}{\Delta^2(l')\Delta^2(l' - l)}. \quad (69)$$

Here $\sum_{l'}'$ means that terms with $l' = l$ or $l' = 0$ are omitted. Taking the continuum limit of Eq. 69, just as we did for Eq. 65 and keeping in mind that μ in this expression is given in units of $1/ag^2$ (*cf.* Section 4), one recovers the corresponding continuum expression of Ref. [23] for $N_c = 2$. In the section on our numerical results we compare our lattice results for the field intensity to Eq. 69.

We now compute the initial kinetic energy of the scalar field Φ in lattice perturbation theory. This can also be checked against our lattice results in weak coupling and provides yet another test of the numerics. In the continuum, using Eq. 47 and Eq. 11, we have

$$p^a p^a = \epsilon^{abc} \epsilon^{ade} \alpha_{\perp i}^{(1),b} \alpha_{\perp i}^{(2),c} \alpha_{\perp j}^{(1),d} \alpha_{\perp j}^{(1),e}, \quad (70)$$

with $i = 1, 2; j = 1, 2$. On the lattice, writing

$$\alpha_{\perp i}^{(1),b} \alpha_{\perp i}^{(1),c} \longrightarrow \sum_n \left\{ (\alpha_{\perp}^{(1),b} \alpha_{\perp}^{(2),c})_{j,\hat{n}} + (\alpha_{\perp}^{(1),b} \alpha_{\perp}^{(2),c})_{j,-n,\hat{n}} \right\}, \quad (71)$$

and using $\alpha_{j,\hat{n}}^{(i)} = (\Lambda^{(i)}(x_j + a\hat{n}) - \Lambda^{(i)}(x_j))/a$

$$\alpha_{j,\hat{n}} = -\frac{\mu}{N} \sum_{\vec{k}} \frac{(\exp(i l_n) - 1) \eta_l}{\Delta(l)} e^{2\pi i \vec{k} \cdot \vec{x}_j}, \quad (72)$$

we have (after Gaussian averaging over η 's)

$$p^a p^a = 6 \left(\frac{\mu}{N} \right)^4 \sum_{n,n'} \left[\left(\sum_{\vec{k}} \frac{\sin(l_n) \sin(l_{n'})}{\Delta^2(l)} \right)^2 + 16 \left(\sum_{\vec{k}} \frac{\sin^2(\frac{l_n}{2}) \sin^2(\frac{l_{n'}}{2})}{\Delta^2(l)} \right)^2 \right]. \quad (73)$$

Let us take a look at the continuum limit of this expression. For $n \neq n'$, the first term vanishes. For $n = n'$, this term is $\propto \mu^4 \log^2(L/a)$; it is logarithmically divergent in the infrared. The second term is infrared safe for all n, n' . Hence

$$p^a p^a \longrightarrow A + B \log^2(L/a), \quad (74)$$

where A and B are constants which may be determined from Eq. 73.

Thus far we have not specified precisely what the lattice expansion parameter is. In the continuum, perturbation theory is applicable when $\alpha_S \mu/k_t \ll 1$. In Ref. [43] the lattice expansion parameter for a single nucleus was estimated numerically to be $g^2 \mu L$. That this is also the case here can be seen from Eqs. 56 and 68.

Finally, the reader may have noted that our lattice perturbation theory results were computed at $\tau = 0$. As noted in section 2, in weak coupling the spatial and temporal distributions factorize. The spatial distributions of the high momentum modes are therefore completely specified at $\tau = 0$.

References

- [1] see for instance, the proceedings of *Quark Matter 96*, *Nucl. Phys.* **A610** (1996).
- [2] K. Kajantie, P. V. Landshoff, and J. Lindfors, *Phys. Rev. Lett.* **59** (1987) 2527.
- [3] K. J. Eskola, K. Kajantie, and J. Lindfors, *Nucl. Phys.* **323** (1989) 37.
- [4] J.-P. Blaizot and A. H. Mueller, *Nucl. Phys.* **B289** (1987) 847.
- [5] X.-N. Wang, *Phys. Rep.* **280** 287 (1997).
- [6] K.. Geiger, *Phys.Rep.* **258** 237 (1995).
- [7] M. Plumer, M. Gyulassy, and X.-N. Wang, *Nucl. Phys.* **A 590** (1995) 511c.
- [8] K. J. Eskola, K. Kajantie, and P. V. Ruuskanen, *Eur. Phys. J.* **C1** (1998) 627.

- [9] K. J. Eskola, *Comments in Nucl. and Part. Phys.* **22** (1998) 185.
- [10] R. Venugopalan, *Comments in Nucl. and Part. Physics*, **22** (1998) 113.
- [11] K. J. Eskola, V. J. Kolhinen, and P.V. Ruuskanen, hep-ph/9802350.
- [12] S. Kumano and K. Umekawa, hep-ph/9803359.
- [13] L. V. Gribov, E. M. Levin, and M. G. Ryskin, *Phys. Rep.* **100** (1983) 1.
- [14] A. H. Mueller and J. Qiu, *Nucl. Phys.* **B268** (1986) 427.
- [15] M. Luo, J. Qiu, and G. Sterman, *Phys. Rev.* **D49** (1994) 4493; **50** (1994) 1951;
J. Qiu and G. Sterman, hep-ph/9610476.
- [16] L. McLerran and R. Venugopalan, *Phys. Rev.* **D49** 2233 (1994); **D49** 3352
(1994); **50** 2225 (1994).
- [17] A. Ayala, J. Jalilian–Marian, L. McLerran and R. Venugopalan, *Phys. Rev.* **D52**
(1995) 2935; it *ibid.*, **D53** (1996) 458.
- [18] J. Jalilian–Marian, A. Kovner, L. McLerran and H. Weigert, *Phys. Rev.* **D55**
5414 (1997).
- [19] J. Jalilian–Marian, A. Kovner, A. Leonidov and H. Weigert, *Nucl. Phys.* **B504**
(1997) 415; hep-ph/9807462.
- [20] J. Jalilian–Marian, A. Kovner, and H. Weigert, hep-ph/9709432.
- [21] Yu. V. Kovchegov, *Phys. Rev.* **D54** 5463 (1996); **D55** 5445 (1997).
- [22] E.A. Kuraev, L.N. Lipatov and Y.S. Fadin, *Zh. Eksp. Teor. Fiz* **72**, 3 (1977)
(*Sov. Phys. JETP* **45**, 1 (1977)); I.A. Balitskii and L.N. Lipatov, *Sov. J. Nucl.*
Phys. **28** 822 (1978); G. Altarelli and G. Parisi, *Nucl. Phys.* **B126** 298 (1977);
Yu.L. Dokshitzer, *Sov.Phys.JETP* **46** 641 (1977).

- [23] A. Kovner, L. McLerran and H. Weigert, *Phys. Rev* **D52** 3809 (1995); **D52** 6231 (1995).
- [24] M. Gyulassy and L. McLerran, *Phys. Rev.* **C56** (1997) 2219.
- [25] Y. V. Kovchegov and D. H. Rischke, *Phys. Rev.* **C56** (1997) 1084.
- [26] S. G. Matinyan, B. Müller and D. H. Rischke, *Phys. Rev.* **C56** (1997) 2191; *Phys. Rev.* **C57** (1998) 1927.
- [27] J. D. Bjorken, *Phys.Rev.* **D27** 140 (1983).
- [28] J. Sollfrank, P. Houvinen, M. Kataja, P. V. Ruuskanen, M. Prakash and R. Venugopalan, *Phys. Rev.* **C55** 392 (1997).
- [29] J. F. Gunion and G. Bertsch, *Phys. Rev.* **D25** (1982) 746.
- [30] J. Ambjørn and A. Krasnitz, *Phys. Lett.* **B362** 97 (1995); hep-ph/9705380.
- [31] G. D. Moore, *Nucl. Phys.* **B480** 657 (1996).
- [32] A. Krasnitz and R. Venugopalan, hep-ph/9706329, in proceedings of *3rd International Conference on the Physics and Astrophysics of the Quark Gluon Plasma*, March 17th–21st, Jaipur, India.
- [33] A. H. Mueller, Y. Kovchegov, and S. Wallon, *Nucl. Phys.* **B507** (1997) 367.
- [34] A. H. Mueller and Y. Kovchegov, *Nucl. Phys.* **B529** (1998) 451-479.
- [35] A. H. Mueller, *Nucl. Phys.* **B415** (1994) 373.
- [36] A. H. Mueller and B. Patel, *Nucl. Phys.* **B425** (1994) 471.
- [37] A. Makhlin and E. Surdutovich, *Phys. Rev.* **C58** (1998) 389.
- [38] I. Balitskii, hep-ph/9807434, hep-ph/9808215.

- [39] M. Gyulassy and X.-N. Wang, *Nucl. Phys.* **420** (1994) 583.
- [40] K. J. Eskola, B. Müller, and X.-N. Wang, *Phys. Lett.* **B374** (1996) 20.
- [41] A. Makhlin, hep-ph/9608261.
- [42] J. Kogut and L. Susskind, *Phys. Rev.* **D11** 395 (1975).
- [43] R. V. Gavai and R. Venugopalan, *Phys. Rev.* **D54** 5795 (1996).
- [44] L. McLerran and R. Venugopalan, *Phys. Lett.* **B424** (1998) 15.
- [45] A. Krasnitz, *Nucl. Phys.* **B455** 320 (1995).
- [46] M. Creutz and A. Goksch, *Phys. Rev. Lett.* **63** (1989) 9.
- [47] A. Krasnitz and R. Venugopalan, to be published.
- [48] U. Heinz, C.R. Hu, S. Leupold, S.G. Matinian and B. Müller, *Phys. Rev.* **D55** 2464 (1997).
- [49] T. S. Biro, C. Gong, B. Müller and A. Trayanov, *Int. J. Mod. Phys.* **C5** 113 (1994).
- [50] S. A. Bass, B. Müller and W. Pöschl, nucl-th/9808011; B. Müller and W. Pöschl, nucl-th/9808031.
- [51] Y. Kovchegov, private communication.
- [52] F. Karsch and H. W. Wyld, *Phys. Rev.* **D35** (1987) 2518.
- [53] M. Testa, hep-ph/9807204.
- [54] C. L. Basham, L. S. Brown, S. D. Ellis, S. T. Love, *Phys. Rev.* **D17** (1978); 2298; *ibid.*, **D 19** (1979) 2018.

- [55] A. Krasnitz and R. Venugopalan, hep-ph/9808332, in proceedings of *3rd international workshop on continuous advances in QCD*, Mpls., MN, April 16th–19th, 1998.
- [56] W. Press, B.P. Flannery, S.A. Teukolsky, and W.T. Wetterling, *Numerical Recipes in C*, Cambridge University Press (1989).
- [57] J.E. Mandula and M. Ogilvie, *Phys. Lett.* **B 248** (1990) 156.